(2)

Dr. 953

DOE/SF/10542-T1
(DE82014662)

DIRECT EXPANSION SOLAR COLLECTOR AND HEAT PUMP

Final Report

May 1982

Work Performed Under Contract No. AC03-79SF10542

Sigma Research, Inc.
Richland, Washington

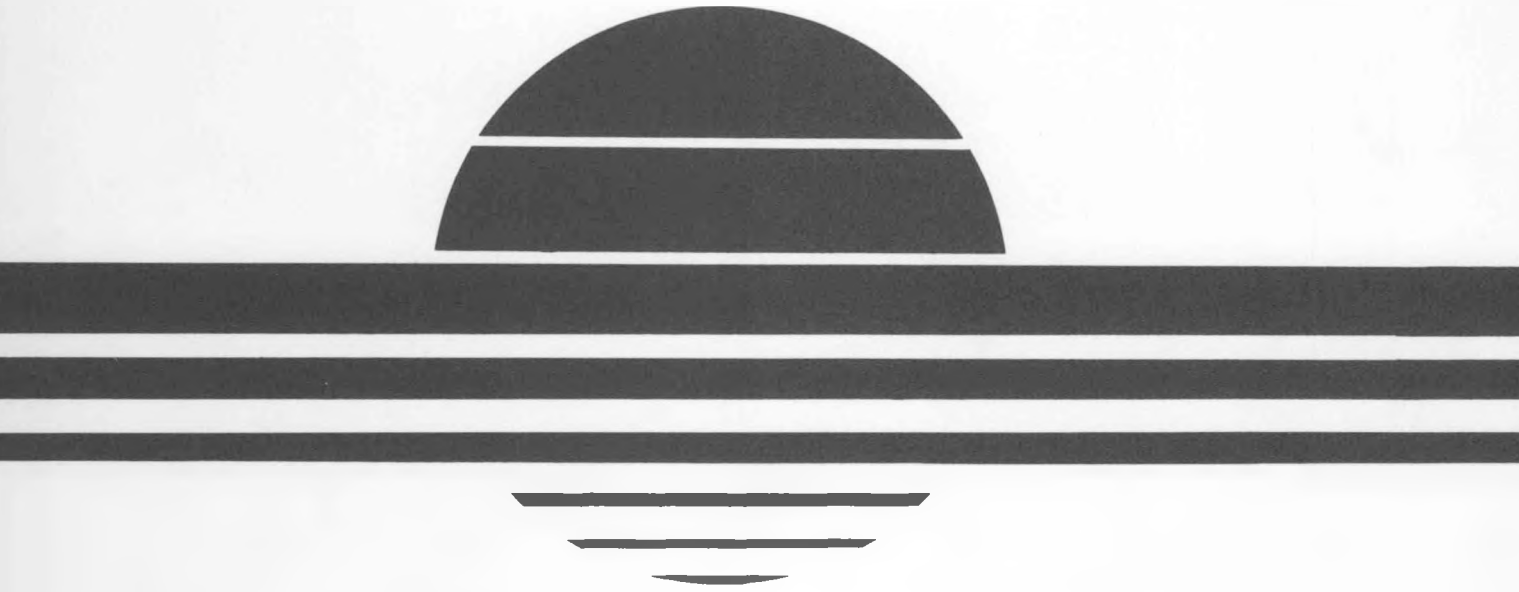

U.S. Department of Energy

Solar Energy

DOE/SF/10542-T1
(DE82014662)
Distribution Category UC-59c

DIRECT EXPANSION SOLAR COLLECTOR AND HEAT PUMP

Final Report

May 1982

Contract DE-AC03-79SF10542

Prepared by

Sigma Research, Inc.
Richland, Washington

CONTENTS

FIGURES

TABLES

Section 1

INTRODUCTION

Sigma Research, Inc., has developed a solar heating system that promises high efficiency and low installed cost. The system is a hybrid heat pump/solar collector combination in which solar collectors replace the outside air heat exchanger found in conventional air-to-air heat pump systems. The solar panels ordinarily operate at or below ambient temperature, eliminating the need to install the collector panels in a glazed and insulated enclosure.

Solar energy absorbed by exposed panels directly vaporizes the refrigerant fluid. The resulting vapor is compressed to higher temperature and pressure; then, it is condensed to release the heat absorbed during the vaporization process. In the absence of solar input, the panel temperature will drop, and significant amounts of energy will be extracted from the ambient air by convection, radiation, and condensation of moisture.

The remainder of this report provides detailed information on the design, operation, control, testing, and modeling of the Sigma system. The direct-expansion collector design is described and compared with other flat-plate collector designs in Section 2. Section 3 contains an analysis of its operation and presents models that allow optimization of the design with respect to certain of its parameters. Section 4 addresses control and monitoring of the demonstration system. Section 5 describes the tests conducted with the demonstration system, points out areas where difficulties arose, and suggests additional work. Section 6 contains modeling of the entire heat pump system, including predicted performance and costs, and makes economic comparisons with conventional flat-plate collector systems. Software listings of certain modeling programs are presented in Appendices A through C.

Section 2

DESIGN DESCRIPTION/RATIONALE

DESIGN LIMITATIONS OF EXISTING SOLAR COLLECTION SYSTEMS

The solar collector system investigated by Sigma Research, Inc., is the result of a detailed assessment of the present status of solar heating and cooling hardware. One of the most obvious conclusions of this study is that the costs of present solar installations are quite high--beyond the economic means of a significant fraction of the population. Solar collectors available today cost from $8 to $23 per square foot, and installation charges can double this expense.

Basic units are expensive because highly effective thermal packages must be used to absorb solar flux and minimize losses by conduction, convection, and radiation. In a typical flat-plate collector (shown in Figure 1), two glass or plastic cover sheets impede convective and radiative heat loss via the front face, while an insulation package from 5-cm to 10-cm thick is used as a backing. Generally, the collector is a copper or aluminum sheet with a black surface to absorb solar energy and periodic water-flow channels to transfer heat from the panel to a water storage tank or water/air heat exchanger. Each collector must be sealed within a waterproof containment shell.

The resulting unit is heavy, bulky, and expensive. In addition, its net collection efficiency is relatively poor when the panel temperature is substantially above that of ambient air. For example, the performance of the commercially available collector shown in Figure 2 indicates an efficiency of

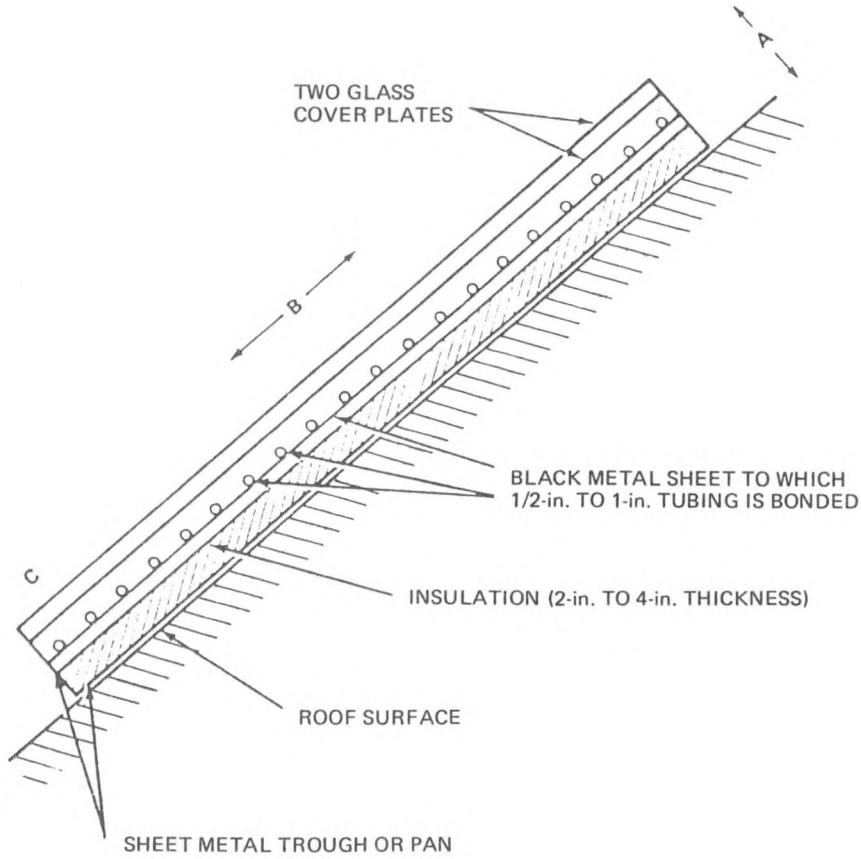

NOTES: ENDS OF TUBES MANIFOLDED TOGETHER. ONE TO THREE GLASS COVERS, DEPENDING ON CONDITIONS.

DIMENSIONS: THICKNESS (DIRECTION "A") 3 in. TO 6 in.; LENGTH (DIRECTION "B") 4 ft TO 20 ft; WIDTH (DIRECTION "C") 10 ft TO 50 ft. SLOPE DEPENDENT ON LOCATION AND WINTER-SUMMER LOAD COMPARISON.

Figure 1. Solar Collector for Residential Heating and Cooling. (Diagrammatic sketch of one alternative.)

20% to 50% when the ambient air temperature is 30°F and the panel temperature is 130°F. Collection efficiency is lowest when the solar input is low--as is often the case under winter conditions. The dramatic reduction in solar input on a cloudy day is apparent in the data of Beckman and Duffy,[1], which are reproduced in Figure 3.

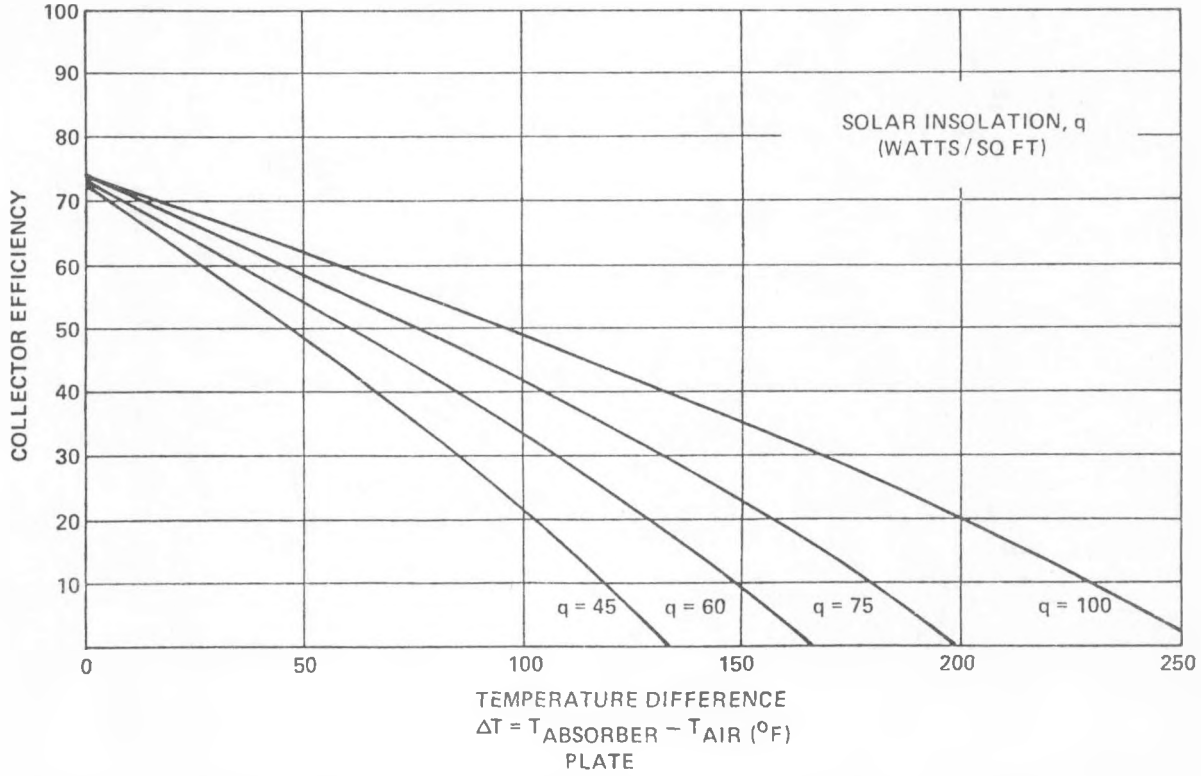

Figure 2. Typical Flat-Plate Collector Efficiencies (Air = 50°F).

In constrast to existing solar collectors, an optimum collector would have the following characteristics:

- Low cost,
- High collection efficiency,
- Rugged construction,
- Low weight, and
- Minimum need for skilled labor in installation.

The hybrid solar collector system investigated under Contract DE-AC03-79SF10542 satisfies many of these requirements.

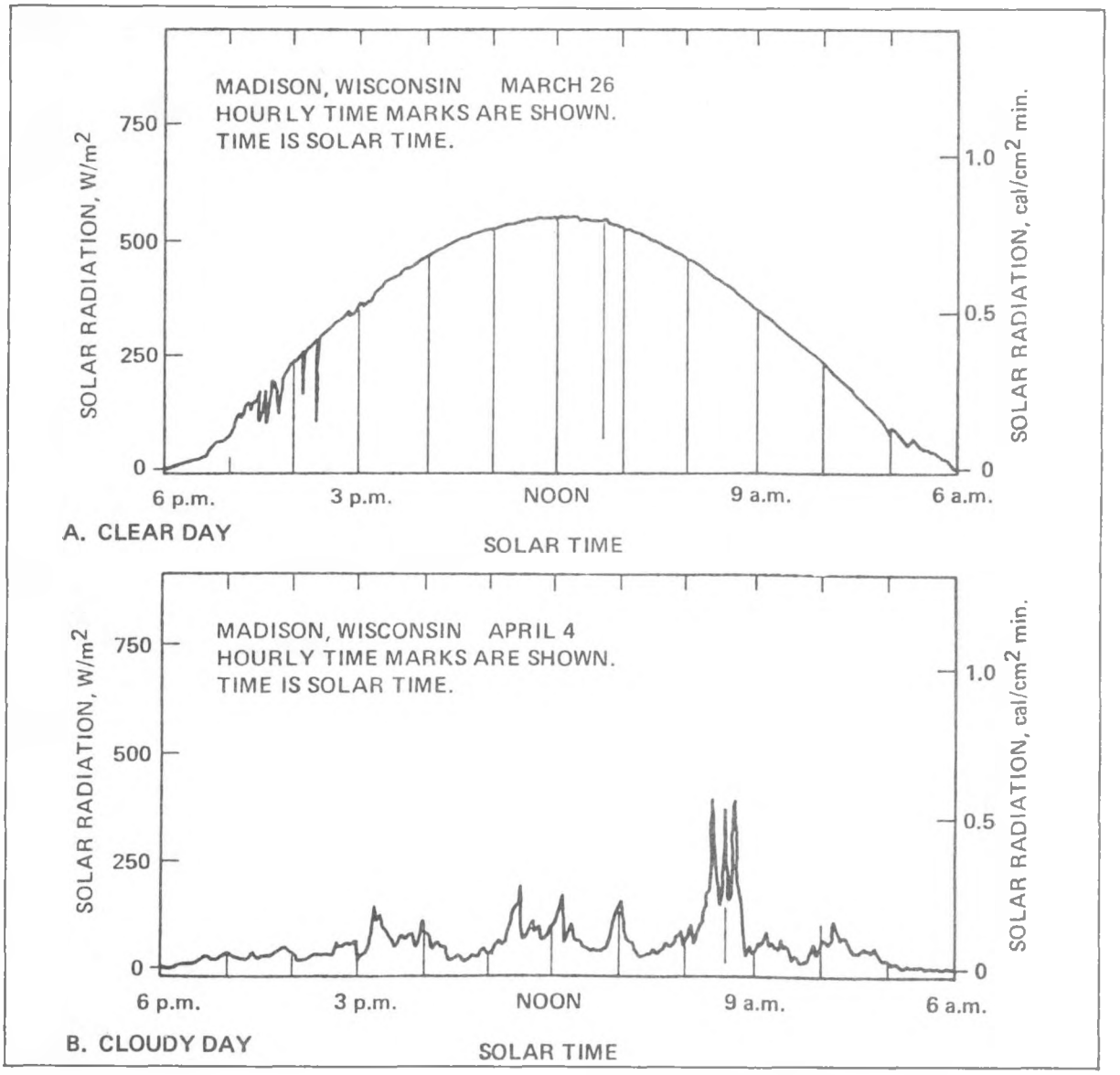

Figure 3. Total (Beam + Diffuse) Solar Radiation on a Horizontal Surface Versus Time.

SIGMA RESEARCH COLLECTOR

The design of the Sigma Research collector is radically different from existing flat-plate collectors and, to our knowledge, is unique. Heat pump/collector combinations have been considered previously, but all have been isolated from the panels by a pumped-water loop and/or thermal storage

tank[2]. Figures 4 and 5 are conceptual drawings of a collector array installed on a residence and a cross section through a single collector element, respectively. Figure 6 is a representative refrigerant circuit for a system that incorporates both heating and cooling. Figure 7 is a photograph of a prototype heating-only research unit.

The Sigma collector incorporates an array of bare flat-plate panels that are connected directly to the heat pump. That is, the panels do not contain water but are used as the inlet heat exchanger for the heat pump system; refrigerant is directly vaporized or condensed within the collector tubes. The collectors have been left totally exposed intentionally so that additional heat can be collected or lost by convection to ambient air (free convection or wind) and by radiation heat transfer. That is, the collectors are operated somewhat below ambient air temperature for heating and considerably above it for cooling. In this manner, the large thermal loss of a

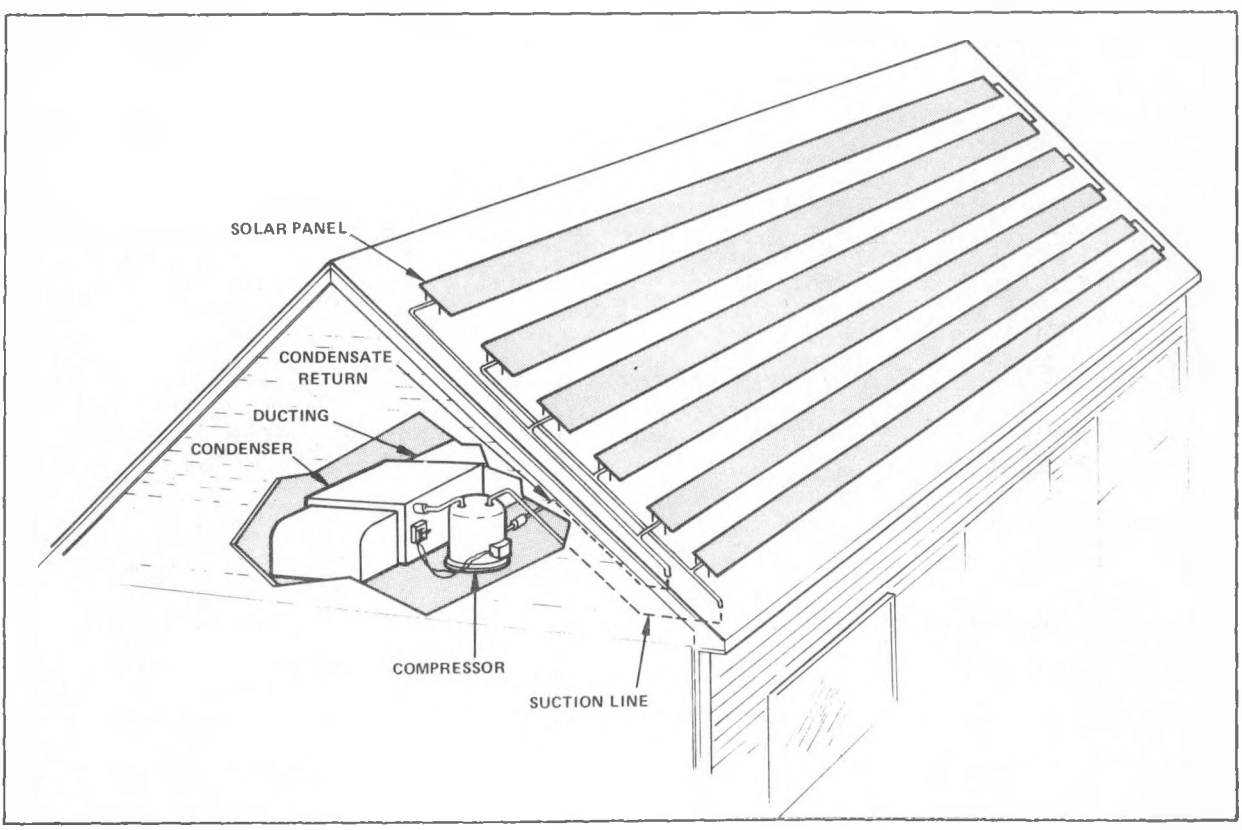

Figure 4. Diagram of Major Components of Installed Solar Panel/Heat Pump System.

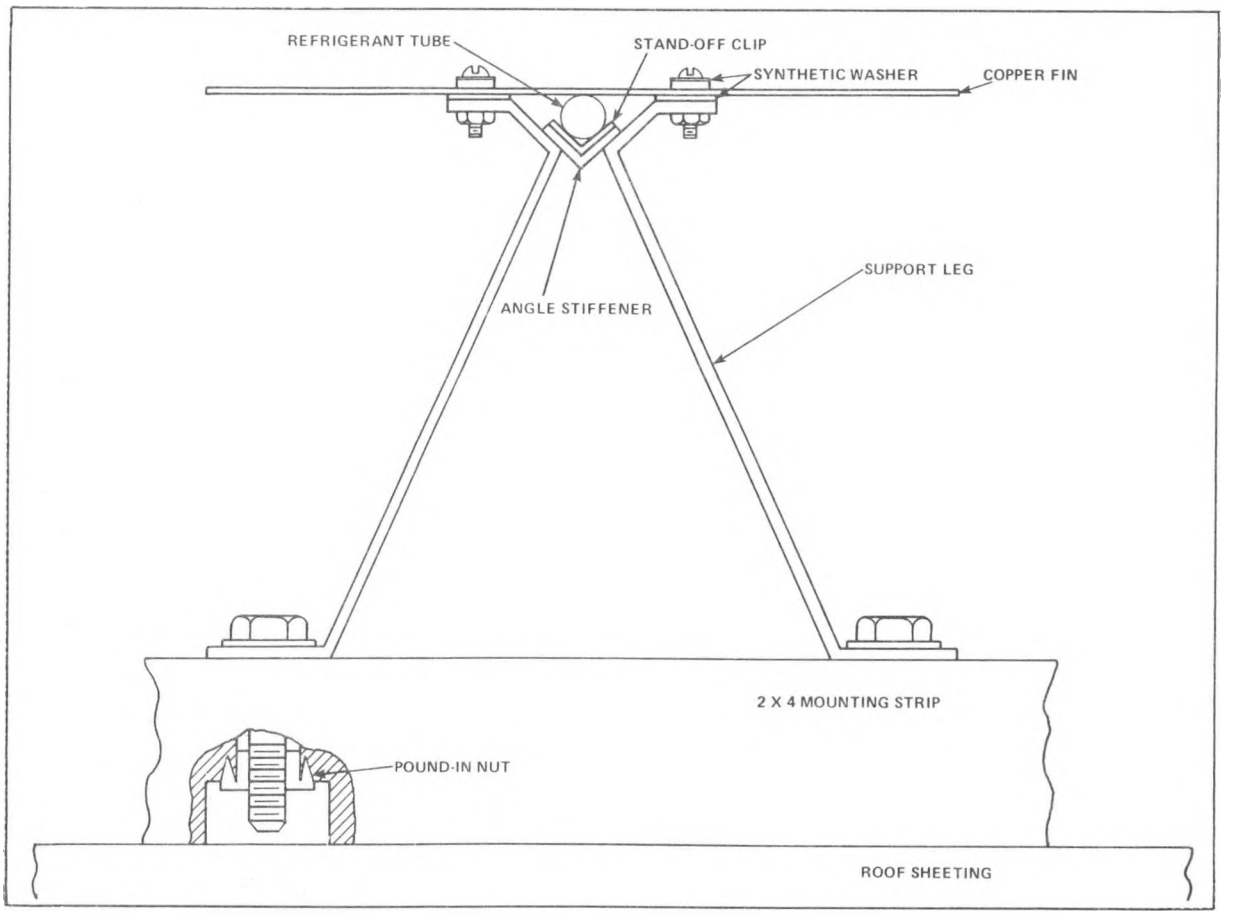

Figure 5. Cross-Section of Collector at one of Periodic Mounting Strips.

typical flat plate collector (Figure 1) is eliminated and heat is actually absorbed from the surroundings, while the supplementary air conditioning function helps to reduce buy-back time in those cases where summer air conditioning is needed. Even under overcast conditions, the panel will collect both solar and air heat; and under rainy conditions, the output is significant due to the high heat capacity of water and the very effective heat transfer from splashing droplets.

To develop usable heat from the vaporized refrigerant, vapor is pumped to a higher temperature and pressure by a hermetic compressor; then, it is condensed in a refrigerant-to-air or refrigerant-to-water heat exchanger for direct use or storage. The resulting condensate is stored in a liquid receiver and ultimately reused in the solar collector via an expansion valve and liquid refrigerant distribution network.

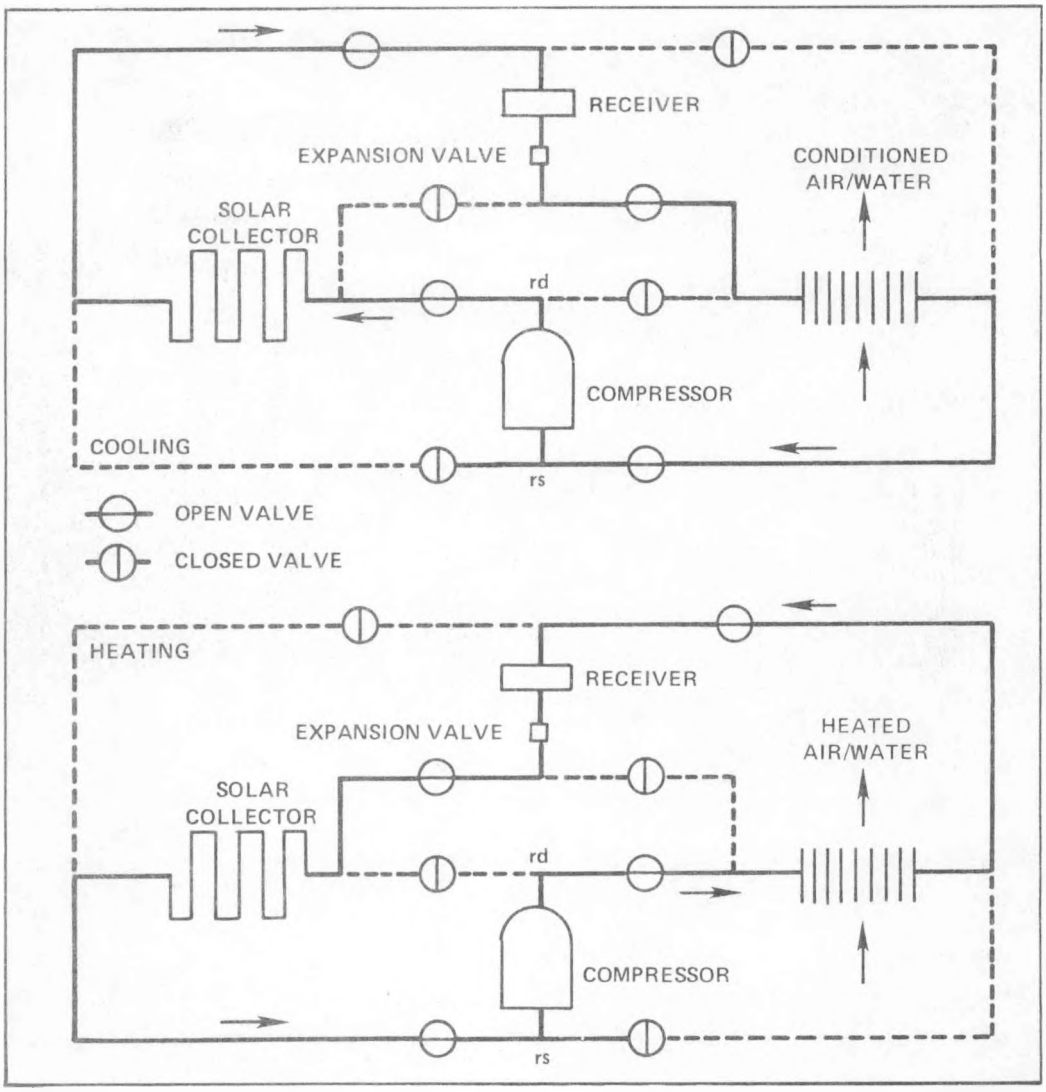

Figure 6. Representative Refrigerant Circuit for Hybrid Solar Heating and Cooling System. (In this configuration, eight solenoid valves ensure correct refrigerant flow direction in circuit and in collector. Collector/compressor combination can couple directly to building air system or indirectly via storage tank.)

The requirement to produce hot air or water is eliminated from the distributed solar array and assigned to a centralized vapor compressor, resulting in considerable savings in collector construction and overall system capital costs. In addition, since the boiling refrigerant within the panels will not freeze, there is no need for a water-glycol intermediate pumped loop. Typical refrigerants of interest include R-12 and R-22, both of

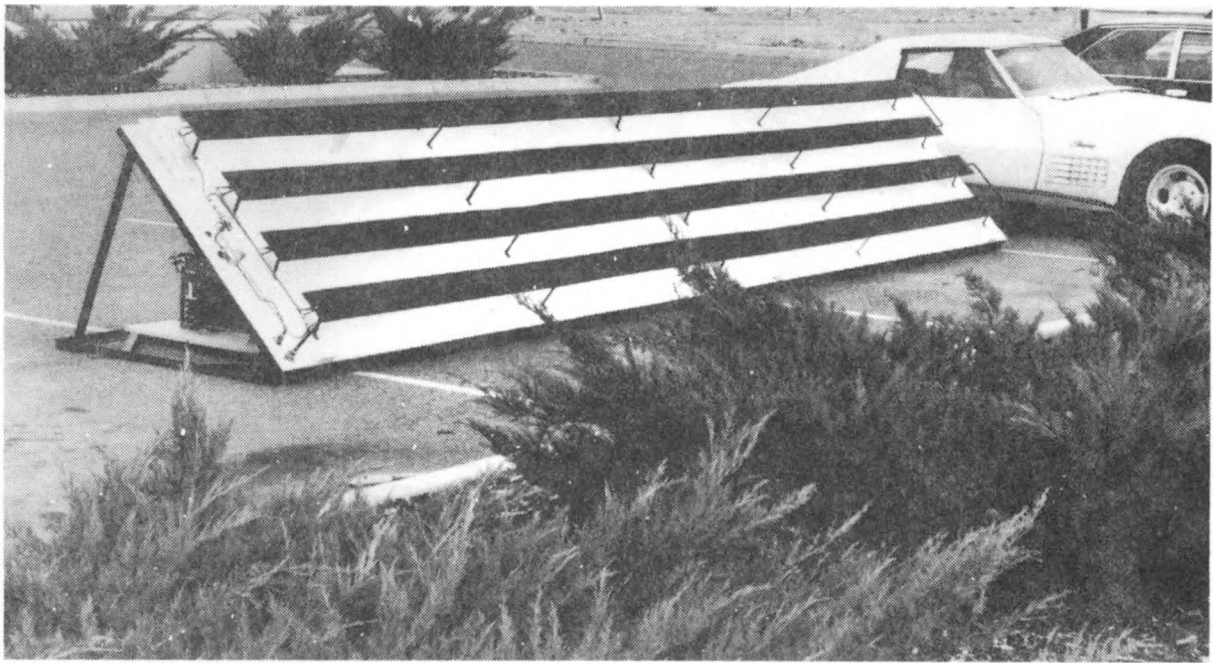

Figure 7. Prototype Direct-Expansion Heat Pump Solar Panel (80 ft^2).

which are extensively used in heat pumps, refrigerators, and air conditioners. Of course, care must be taken in selecting compressor and discharge heat exchanger capacities to ensure that compressor input power is relatively small compared to heat output; i.e., that the system coefficient of performance (COP) is satisfactory. This is discussed further in Section 6, System Analysis and Optimization.

The collectors are mounted to the roof with an angle bracket system (see Figure 5). The brackets and 2 x 4 mounting strips are located at approximately 3-m (10-ft) intervals, and a total collector element may be up to 12 meters (40 feet) long; however, as the collectors are made longer, provision must be made for differential expansion. The space between the collectors and the roof is approximately equal to the total fin width. This allows the collectors to absorb a considerable amount of reflected solar radiation from the rear face of the flat plate and allows air to flow over the rear surface.

As a compromise between minimizing roof area and maximizing solar collection from the rear, the individual flat plates in the two prototypes are separated by a distance equal to their width (see Figure 4); therefore,

spacing from roof ≃ spacing between panels ≃ panel width.

The roof behind the panels must be painted white, or a reflective surface must be used to ensure maximum solar input to the rear surface of each panel.

The panels are constructed of sheet copper from 22 ga to 30 ga, are approximately 10 cm to 15 cm wide (4 to 6 inches), and each is soldered to a centrally located refrigerant evaporator tube as shown in Figure 5. To ensure stability under severe wind conditions, this flat plate/tube structure must be reinforced by a steel angle stiffener that runs the length of each collector panel (see Figure 5). This stiffener must be electrochemically isolated from the copper to minimize corrosion of the steel; this is accomplished using paint and a plastic liner.

THERMAL STORAGE

The mass and volume of a thermal storage installation are minimized by arranging for the storage of latent heat of melting in a suitable low-melting compound. Some preliminary screening of candidate materials was accomplished, and Table 1 lists materials having melting points or water of crystallization changes in the range between 29°C and 60°C (84°F to 140°F). Some cost information is also shown.

DESIGN SUMMARY

In summary, the solar collector is an array of exposed flat plates used as the outdoor heat exchanger of a heat pump. The absence of insulation and cover glass lowers manufacturing costs and produces a collector that is lightweight, rugged, and relatively invulnerable to acts of vandalism such

Table 1

CANDIDATE MATERIALS

Material	Cost per lb	Melting Point (°C)	Chemical Formula	Density (g/cc)
Ammonium Iron Sulfate	–	39-41	$NH_4Fe(SO_4)_2 \cdot 12H_2O$	1.71
Calcium Chloride, hexahydrate*	$0.028	29.92 -4H O @ 30°C	$CaCl_2 \cdot 6H_2O$	1.71
Calcium Nitrate, tetrahydrate	–	39.7–42.7	$Ca(NO_3)_2 \cdot 4H_2O$	1.82–1.90
Calcium Nitrate, trihydrate	–	51.1	$Ca(NO_3)_2 \cdot 3H_2O$	–
Ferric Chloride	NL	56	$FeCl_3 \cdot 2\text{-}½H_2O$	1.82
	NL	37	$FeCl_3 \cdot 6H_2O$	–
Ferric Nitrate	NL	35	$Fe(NO_3)_3 \cdot 6H_2O$	1.684
	NL	47.2	$Fe(NO_3)_3 \cdot 9H_2O$	–
Ferrous Nitrate	NL	60.5	$Fe(NO_3)_2 \cdot 6H_2O$	–
Magnesium Chlorate	NL	35	$Mg(ClO_3)_2 \cdot 6H_2O$	1.8
Pyrophosphoric Acid	–	38	$H_4P_2O_7$	–
Potassium Triiodide	–	31	$KI_3 \cdot ½H_2O$	3.498
Phosphoric Acid	$0.145	42.35	H_3PO_4	1.864
Potassium Subphosphate	–	40	$K_2PO_3 \cdot 4H_2O$	–
Potassium Pyrophosphate Tetrabasic	$0.41			
Potassium Monosulfide	–	60	$K_2S \cdot 5H_2O$	
Sodium Acetate Trihydrate*	$0.355	58	$NaC_2H_3O_2 \cdot 3H_2O$	1.45
Sodium Metaborate	$0.188	57	$NaBO_2 \cdot 4H_2O$	–
Sodium Carbonate Decahydrate*	$0.028	32.5-34.5	$Na_2CO_3 \cdot 10H_2O$	1.44
Sodium Carbonate Heptahydrate*	$0.028	-1H O @ 32°C	$Na_2CO_3 \cdot 7H_2O$	1.51
Sodium Lithium Sulfate	–	-6H O @ 50°C	$Na_3Li(SO_4)_2 \cdot 6H_2O$	2
Sodium Metaphosphate*	$0.25	53 -6H O @ 50°C	$Na(PO_3)_3 \cdot 6H_2O$	–
Sodium Orthophosphate, mono-H (Dibasic)	–	-5H O @ 48.1°C	$Na_2HPO_4 \cdot 7H_2O$	1.679
Sodium Orthophosphate, mono-H (Dibasic)	–	-5H O @ 35.1°C	$Na_2HPO_4 \cdot 12H_2O$	1.52
Sodium Orthophosphite, di-H	–	42	$NaH_2PO_3 \cdot 2\text{-}½H_2O$	–
Sodium Orthophosphite, mono-H	–	53	$Na_2HPO_3 \cdot 5H_2O$	–
Sodium Metasilicate*	$0.144	40-48	$NaSiO_3 \cdot 9H_2O$	–
Sodium Sulfate Decahydrate	$0.033	32.38	$Na_2SO_4 \cdot 10H_2O$	1.464
Sodium Hydrogen Sulfate, mono-H	$0.069	58.54	$NaHSO_4 \cdot H_2O$	2.103
Sodium Thiosulfate, pentahydrate	$0.083	40-45	$Na_2S_2O_3 \cdot 5H_2O$	1.729
Tin Chloride, dihydrate	–	37.7	$SnCl_2 \cdot 2H_2O$	2.71
Zinc Nitrate, trihydrate*	$0.34	45.5	$Zn(NO_3)_2 \cdot 3H_2O$	–
Zinc Nitrate, hexahydrate*	$0.34	36.4	$Zn(NO_3)_2 \cdot 6H_2O$	2.065

*Denotes anhydrous cost.

as thrown rocks. The solar collection efficiency is very high since the collector is operated below air temperature; in fact, a significant component of the heat input is derived from convective flow over the fins. In addition, the collector should operate well under rainy conditions, since it will absorb sensible heat from the impinging rainfall.

The simplicity of the design will allow a home owner to perform most of the installation, and more industrious home owners could actually build the flat-plate collectors. It would be necessary, however, for a plumber or steamfitter to solder all fittings that are subjected to refrigerant pressure.

This hybrid heat pump/collector system is particularly useful and applicable in a cloudy and damp environment, and it appears to be considerably easier and less costly to install than conventional flat-plate collectors.

Section 3

COLLECTOR ANALYSIS AND OPTIMIZATION

COLLECTOR OPERATION

The system collector is basically an exposed, bare, flat plate with a centrally located tube running longitudinally (see Figure 8). The plate is elevated from the backing surface a predetermined distance so that convective and radiative heat transfer can occur over the back surface. The tube contains a two-phase mixture of refrigerant liquid and vapor that extracts heat from the collector plate upon evaporation. In the heating mode, the entire assembly is run somewhat below ambient temperature to ensure that heat is gained, rather than lost, from the ambient air.

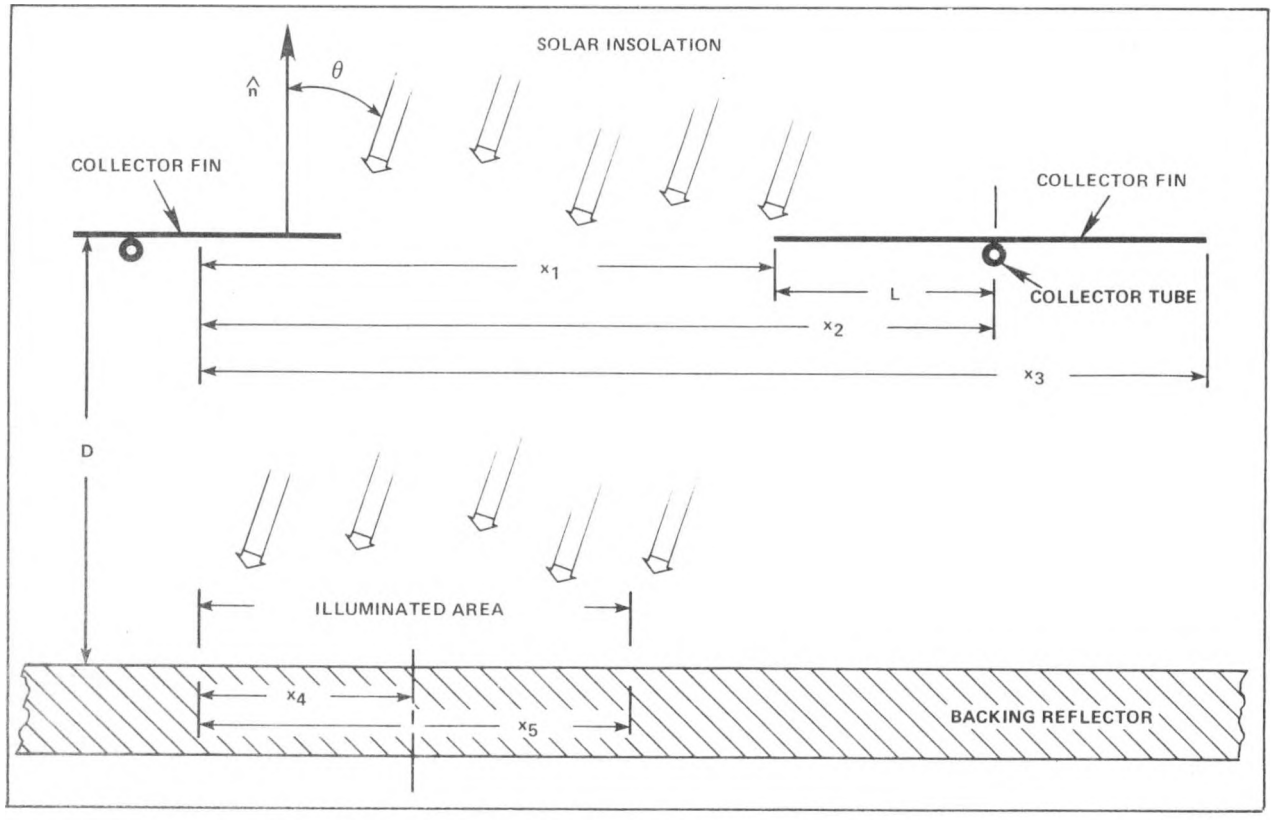

Figure 8. Diagram of Collector Fin-Roof Geometry.

With the exception of the heat transfer phenomena occurring at the rear plate surface, this system is generically similar to conventional flat-plate collectors with regard to thermal modeling. With the collector tube idealized as a thermal node at temperature T_o, for an ambient temperature T_a, the heat input per unit length to the collector tube, Q_ℓ (W/m), may be expressed as

$$Q_\ell = 2\left[T_a - T_o + \frac{\phi_a}{h}\right]\left[hKPt\right]^{1/2} \tanh\left[\left(\frac{hPL^2}{Kt}\right)^{1/2}\right] \qquad 3\text{-}1$$

where:

h = average heat transfer coefficient between the plate and the ambient air,

K = plate thermal conductivity,

L = plate half-width,

t = plate thickness, and

ϕ_a = average absorbed solar flux density (W/m^2).

If heat transfer occurs from the front face only, the parameter $P \equiv 1$; if heat transfer occurs from both sides of the plate, $P \equiv 2$. The average solar flux density in Figure 8 is the arithmetic mean of the front and rear face intensities ϕ_{sf} and ϕ_{sr}. For scoping purposes, ϕ_{sf} is taken as the beam component of terrestrial level solar radiation multiplied by the solar absorptivity of the collector α_{sc},

$$\phi_{sf} = (\alpha_{sc})(\phi_{sb}) \qquad 3\text{-}2$$

while the rear solar intensity ϕ_{ar} must be obtained from a more detailed analysis of collector geometry and reradiation.

VIEW FACTORS FOR REFLECTION TO BACKSIDE OF SPACED ARRAY

The elevated, spaced-panel design of the heat pump collector allows the panel to absorb significant amounts of reflected solar insolation incident on the backing behind the panels. In addition to surface properties, the percentage of incident energy absorbed by the panel is a function of panel size, spacing, elevation, and incident solar angle with respect to the normal to the backing. For a set fin width and spacing, this percentage increases with increasing elevation from the panel. For aesthetic and construction purposes, however, it is prudent to choose a moderate elevation. For this reason, accurate determination of the radiation heat transfer view factor is essential so that configurations will maximize appearance and performance.

The determination of the relationships that affect the view factor is based on the diffuse-gray surface assumption for the backing surface (reflector). In addition, the large length-to-width ratios common to this collector permit neglect of end effects, thereby reducing the calculation method to a double instead of a triple integral. A further assumption that the incident energy is concentrated within a small solid angle centered about the sun's position permits computation of the required relationship.

The solution procedure begins with the relationship for the view factor between infinite strips of differential width having parallel generating lines--a relationship that is given by

$$dF_{dx_2-dx_4} = \frac{D^2}{2}\left\{\int \frac{dx_4}{\left[D^2 + (x_2 - x_4)^2\right]^{3/2}}\right\} \qquad 3\text{-}3$$

where:

dF = view factor between differential areas,

dx_2 = differential area centered about x_2 (ft),

dx_4 = differential area centered about x_4 (ft), and

D, x_2, x_4 are as shown in Figure 8.

By integrating this relationship twice, it is possible to obtain the expression for a fin and reflector surface of finite width, which is given by

$$F_{x_2-x_4} = \frac{1}{2x5}\left\{\left[D^2 + x_3^2\right]^{1/2} - \left[D^2 + (x_3 - x_5)^2\right]^{1/2} + \left[D^2 + (x_1 - x_5)^2\right]^{1/2} - \left[D^2 + x_1^2\right]^{1/2}\right\} \qquad 3\text{-}4$$

where the terms are as given in Figure 8.

Since one illuminated area will "see" or reflect radiant energy to more than one collector fin, the above relationship for one illuminated area must, in principle, be applied to all opposing collector fins. This summation defines the total percentage of solar energy incident on one surface that is reflected to all the collector fins in the array. Computation of the view factor is accomplished with the computer program VIEW (see Appendix A). This program assumes an infinitely long collector and computes view factors using Hottel's string method and user-specified dimensions:

- Position of the backing,
- Distance along the backing to the lower edge of the collector fin of interest,
- Collector fin width,
- Spacing between collector fins,
- Spacing between collector fins and backing, and
- Position of the sun.

From these data, and based on the assumption that the remainder of the backing is covered with collector fins to a width slightly narrower than that of the backing (fins did not overlap upper or lower edges of backing), VIEW computes various view factors, including those to sunlit and shaded areas of the roof and backing.

SOLAR INPUT MODEL

A model of the total solar heat input to a collector was developed as computer program SINPT (see Appendix B). Parameters in the computation are latitude, time of day, day of the year, atmospheric transmittance, and optical properties of the reflector, roof, and collector fins. The geometry of the collector and resultant view factors are computed using VIEW as a subprogram. Based on the day-of-the-year input by the user, SINPT computes the solar declination using an approximate formula presented by Cooper.[3]

$$D_1 = 23.45 \left[\sin \frac{360(284 + N_1)}{365} \right] \qquad 3\text{-}5$$

where:

D_1 = solar declination (degrees), and

N_1 = day of the year.

Using the solar declination thus computed and the site latitude supplied by the user, sunrise and sunset in local solar time are computed using equations given by Smart.[4]

$$S_8 = 12 - \frac{24}{360} \cos^{-1}[- \tan(L) \tan(D_1)] \qquad 3\text{-}6$$

$$S_9 = 12 + \frac{24}{360} \cos^{-1}[- \tan(L) \tan(D_1)] \qquad 3\text{-}7$$

where:

S_8 = sunrise (local solar time),

S_9 = sunset (local solar time), and

L = site latitude.

Next, the code calculates the local solar times at which the angle of incidence (the angle between the normal to the collector's surface and the sun's rays) is 90°, using the following equations.

$$S_6 = 12 + \frac{24W}{360} \qquad 3\text{-}8$$

$$S_7 = 12 - \frac{24W}{360} \qquad 3\text{-}9$$

$$W = -\cos^{-1}\left\{\frac{[\sin(D_1)\cos(L)\sin(T) - \sin(D_1)\sin(L)\cos(T)]}{[\cos(D_1)\cos(L)\cos(T) + \cos(D_1)\sin(L)\sin(T)]}\right\} \qquad 3\text{-}10$$

where T equals the acute angle between the plane of the collector and the roof.

The code selects the appropriate time period, sunrise to sunset or 90° angle of incidence to 90° angle of incidence, over which to integrate the solar input into the fin. As would be expected, this results in integrations from sunrise to sunset in the winter and from 90° angle of incidence to 90° angle of incidence in the summer.

After selecting the period of integration, SINPT divides it into a number of equal time steps. At the central time in each time step, the code computes the altitude and azimuth of the sun, using the following equations.

$$A_1 = 90 - Z_2 \qquad 3\text{-}11$$

$$B = 180 - \cos^{-1}\left\{\frac{[\sin(D_1) - \sin(L)\cos(Z_2)]}{[\cos(L)\sin(Z_2)]}\right\} \qquad 3\text{-}12$$

$$Z_2 = \cos^{-1}[\sin(L)\sin(D_1) + \cos(L)\cos(D_1)\cos(H)] \qquad 3\text{-}13$$

$$H = \frac{360}{24}(12 - K) \qquad 3\text{-}14$$

where:

A_1 = solar altitude (degrees),

B = solar azimuth (degrees),

Z_2 = zenith angle (degrees), and

K = solar time.

These values, along with user-supplied information on the geometry of the collector, are used by program VIEW, which computes the necessary view factors.

The intensity of the solar radiation reaching the ground is also needed to compute the solar input to the collector. This is a function of time of the year, time of day, and atmospheric transmittance. The extra-terrestrial solar intensity, as a function of day of the year, was modeled as follows:

$$E = 1353 + 44 \cos\left(N_1 \frac{360}{365}\right) \qquad 3\text{-}15$$

where E equals extraterrestrial solar intensity (W/m^2).

The effect of time of day and atmospheric transmittance on the intensity of solar radiation reaching the ground is given by Duffie and Beckman[1] as:

$$E_1 = ER^{[1/\cos(Z_2)]} \qquad 3\text{-}16$$

where:

E_1 = solar intensity at ground level (W/m^2), and

R = atmospheric transmittance.

The contributions of direct, reflected-from-backing, and reflected-from-roof solar radiation to the total solar input to the fin are given by the following equations (3-17).

$$\Delta Q_1 = E_2 A_9 T_1$$

$$\Delta Q_2 = E_2 F_7 R_1 A_9 T_1$$

$$\Delta Q_3 = E_3 (F_9 + F_1) R_2 A_9 T_1$$

$$E_2 = E_1 \cos(M)$$

$$E_3 = E_1 \cos(Z_2)$$

$$M = \cos^{-1}\left\{\sin(D_1)\ \sin(L)\ \cos(T) - \sin(D_1)\ \cos(L)\ \sin(T) + \left[\cos(D_1)\ \cos(L)\ \cos(T) + \cos(D_1)\ \sin(L)\ \sin(T)\right]\ \cos\left[\left(12 - K\right)\frac{360}{24}\right]\right\}$$

where:

ΔQ_1 = increment in solar input from direct radiation,

ΔQ_2 = increment in solar input reflected from backing,

ΔQ_3 = increment in solar input reflected from roof,

E_2 = solar intensity on fin and backing,

E_3 = solar intensity on roof,

A_9 = fin absorptance,

R_1 = backing reflectance,

R_2 = roof reflectance,

F_1 = view factor - front of fin to roof,

F_7 = view factor - rear of fin to backing,

F_9 = view factor - rear of fin to sunlit portion of roof,

T_1 = time increment, and

M = angle of incidence of the sun's rays on the collector surface.

These increments are summed from the starting time to solar noon and resulting sums are doubled to give the total solar inputs over one solar day.

OPTIMIZATION BASED ON SOLAR INPUT AND GEOMETRY

Fin Spacing

Figure 9 illustrates the placement of collector fins and identifies the areas considered in the analysis of the effects of fin width (W), spacing between fins (S), and spacing between fins and backing (D). As the figure shows, some of the sunlight passes between the collector fins and strikes the backing directly. As this solar insolation is reflected from the backing to the undersides of the fins, a portion can be absorbed, providing additional thermal input to the collector.

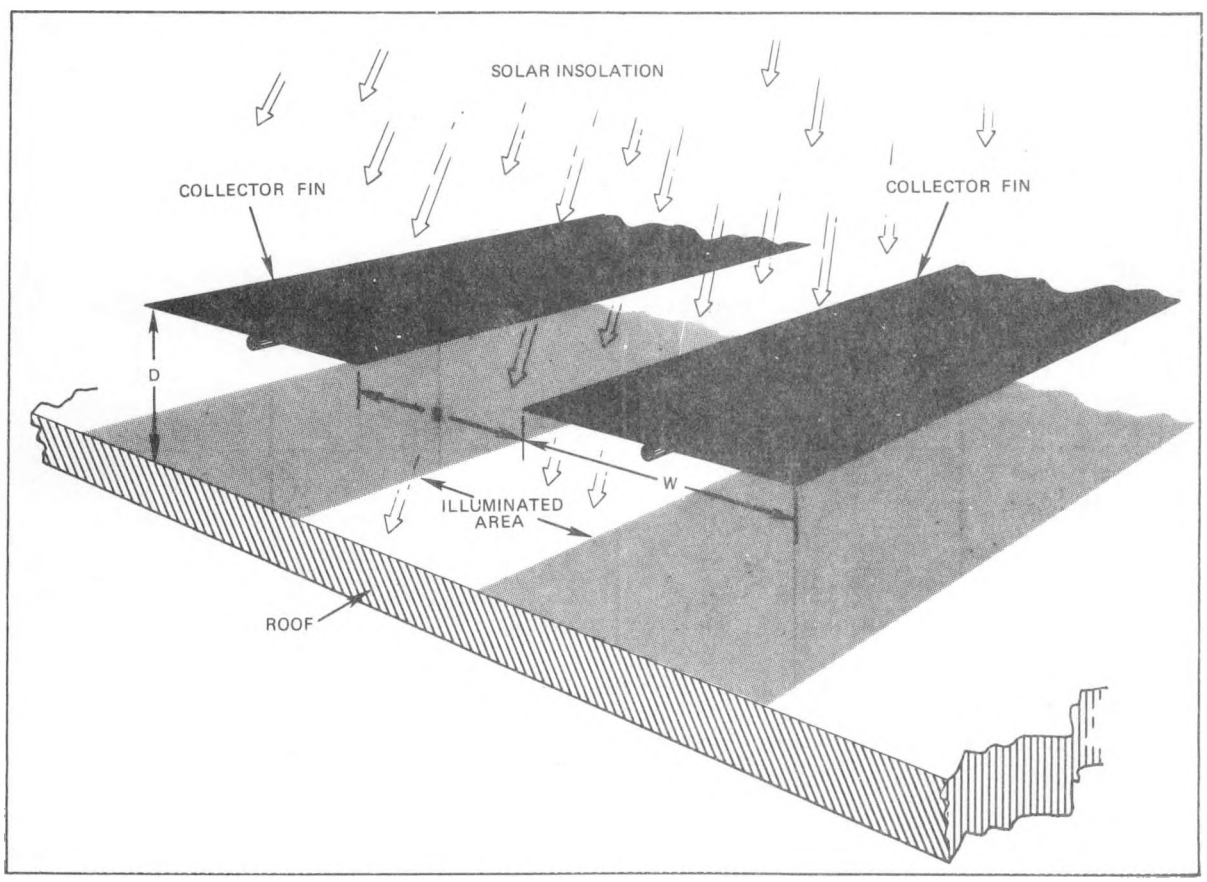

Figure 9. Solar Collector Diagram.

A matrix was prepared (Table 2) to show the ratio of total solar input (Q''_{ST}) to direct solar input (Q''_{SD}) as a function of fin spacing and fin-to-roof separation. The figures are yearly averages for a collector at 45° north latitude and a backing with a reflectance of 0.85. Using this matrix, it was determined that large values of S/W and D/W led to significant increases in solar input to the collector on a watts-per-square-meter-of-fin basis; however, large values of S/W led to low collection efficiencies when solar input was considered on a watts-per-square-meter-of-backing basis.

Table 2

(Q''_{ST}/Q''_{SD})

S/W \ D/W	0.0	0.5	0.75	1.0	1.5	3.0
3.0	1.0	1.34	1.45	1.51	1.59	1.63
1.5	1.0	1.33	1.42	1.46	1.50	1.51
1.0	1.0	1.31	1.38	1.41	1.42	1.42
0.75	1.0	1.29	1.34	1.36	1.36	1.36
0.5	1.0	1.25	1.27	1.28	1.28	1.28
0.0	1.0	1.0	1.0	1.0	1.0	1.0

where:

Q''_{ST} = beam and reflected beam solar input to the fin (W/m^2),

Q''_{SD} = beam solar input to the fin (W/m^2),

W = fin width (cm),

S = spacing between fins (cm), and

D = spacing between fins and backing (cm).

Translated into practicalities, these results indicate that the collector would be quite large for high S/W values. It could conceivably be larger than the available space, and it might detract from or mar the visual aspect of the structure. Similarly, large values of D/W--and the resulting wider separation in fin-to-roof spacing--could also be visually unattractive and could necessitate additional strength in the fin supports, increasing the cost of construction.

For a final determination of optimum values of S/W and D/W, factors such as construction costs (of collector fins, supports, and backing) would have to be considered along with the limitations of the area available and possible visual impacts.

Collector Tilt

Calculations were made to show the direct, reflected, and total beam solar input on three days of the year (days 81, 172, and 355) for a solar-assisted heat pump collector with the following characteristics.

- Latitude - 40° North
- Atmospheric Transmittance - 0.81
- Backing Reflectance - 0.85
- Fin Absorbance - 0.90
- Fin-Spacing to Fin-Width Ratio - 1.5
- Fin-Roof-Separation to Fin-Width Ratio - 1.5

On day 81, which represents a typical spring or fall day, the solar declination is 0°, and the time between sunrise and sunset is 12 hours. On day 172, the sun is in its most northerly declination (approximately 22.5°), and the duration of sunlight is approximately 14 hours, 50 minutes. On day 355, corresponding to the sun's most southerly position, declination is approximately -23.5°, and the sunlight period is approximately 9 hours, 9 minutes (its shortest duration). Figures 10a (day 81), 10b (day 172),

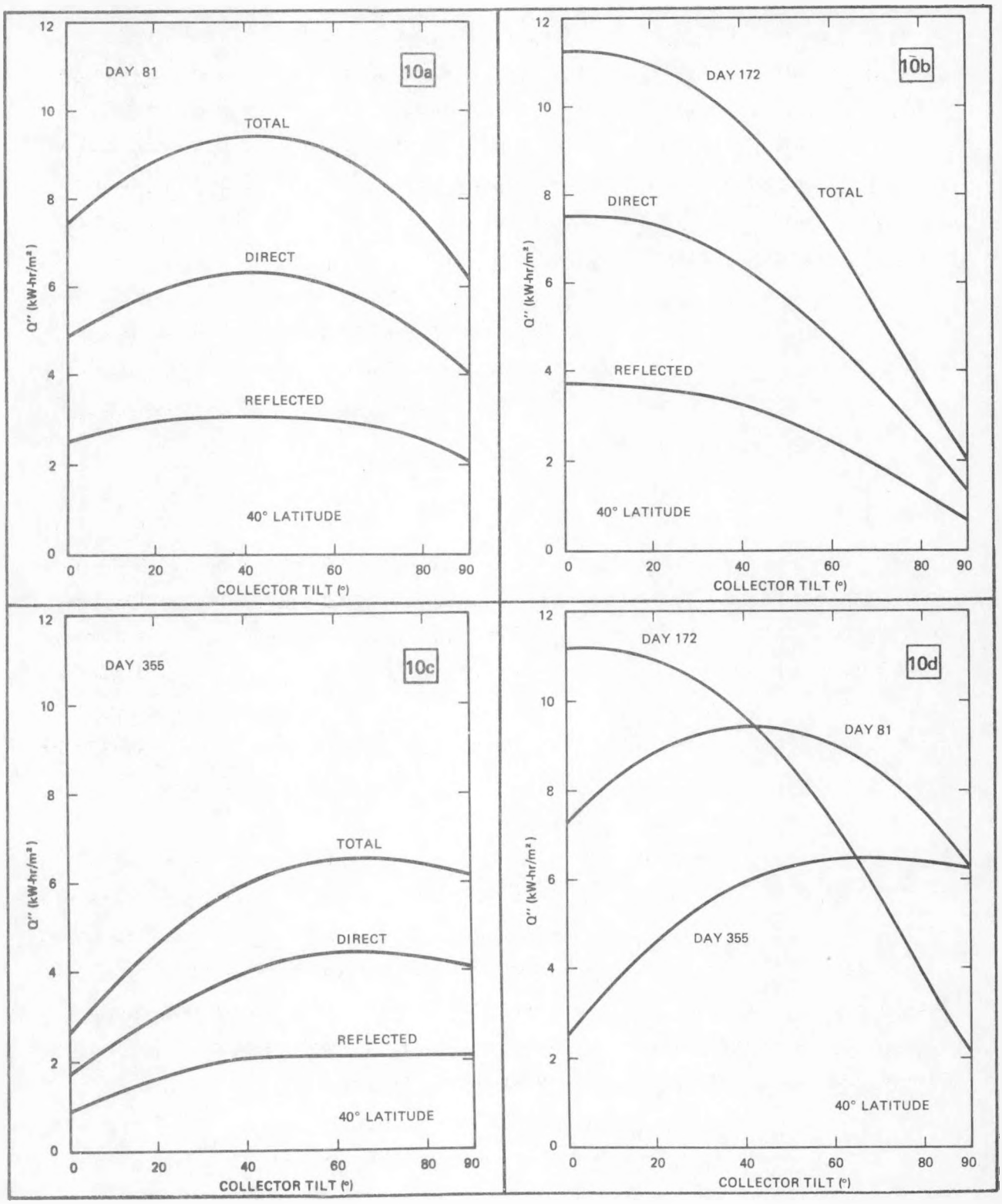

Figure 10. Solar Input Per Square Meter of Fin.

and 10c (day 355) compare the direct, reflected, and total solar input on each of the respective days; and Figure 10d compares the total solar input for the three days examined.

The maximum total solar input occurs at a collector tilt that is approximately the latitude minus the solar declination. The reflected component of solar input, however, is relatively unaffected by small changes in tilt near the optimum position because the view factor between the fins and the illuminated bands on the backing improves as the sunlight deviates from normal incidence on the collector and, simultaneously, its solar intensity decreases. These effects tend to offset each other and cause little or no change in the reflected component.

As Figure 10d indicates, collector tilt produced the greatest effect on day 172. When the solar declination is less than or equal to zero (as on day 81), the collector is exposed to solar radiation from sunrise to sunset regardless of tilt angle. When the declination is positive (as on day 172), however, the sun rises and sets behind the collector and the number of hours of illumination becomes a function of panel tilt. Table 3 correlates the degree of tilt and the hours of illumination for day 172 at 40° north latitude.

Based on these computations, a collector mounted on a south-facing, vertical wall is considered adequate to provide heat during the fall-winter-spring season. Even at angles as low as 25°, solar input on day 355 would be within 80% of maximum value. Moreover, there would be sufficient input during summer to accommodate domestic hot water needs. A wide range of collector tilts, therefore, would be suitable for use with this collector design and would allow flexibility in installation.

Table 3

ILLUMINATION PERIOD AND COLLECTOR TILT FOR DAY 172

Tilt (deg)	Time (hr)
0	14.84
10	13.93
20	13.21
30	12.58
40	12.00
50	11.42
60	10.79
70	10.07
80	9.15
90	7.85

CLIMATOLOGY OF THE HANFORD AREA

Richland is located in South Central Washington on the Columbia River at the mouth of the Yakima River. The Department of Energy Hanford complex lies north and northwest of the city. Records of local weather and climate come from the Hanford Meteorology Station located about 25 miles northwest of Richland.

This section of the state has a very dry climate, relatively mild winters, and warm sunny summers. The Rocky Mountains and the ranges of southern British Columbia protect the inland basin from the more severe winter storms moving southward from Canada. Occasionally, an outbreak of cold air does reach the basin and produces low temperatures or damaging spring or fall freezes. To the west, the Cascade Mountains obstruct the easterly flow of moist air from the Pacific Ocean. Prevailing westerly winds above the mountains are strongest in winter.

Approximately 70% of the 7-inch annual precipitation is received during the six-month period from November through April. In midsummer, it is not unusual for three to six weeks to pass with only a trace of rain. During the winter season, moist air crossing the Cascades and mixing with the colder air of the inland basin results in considerable cloudiness and some fog. Average sky cover during daylight hours is 70-80% in winter; during July and August it is only about 30%.

Some monthly average values of temperatures, wind speeds, and dew points are collected in Table 4. Also appearing in this table are some estimated minor heat inputs computed as described in the following sections. Monthly average insolations at various hours of the day are tabulated in Table 5.

Table 4

CLIMATOLOGICAL DATA FOR RICHLAND AND DERIVED COLLECTOR CHARACTERISTICS*

Parameter	Jan	Feb	Mar	Apr	May	Sep	Oct	Nov	Dec
Mean Temperature (°F)	33.7	40.8	46.4	55.2	62.7	66.6	55.6	43.6	36.9
Mean Minimum Temperature (°F)	23.9	29.5	34.3	40.6	49.0	51.2	42.0	33.4	29.7
Mean Maximum Temperature (°F)	41.4	50.2	58.0	68.3	76.3	81.4	68.4	53.1	43.8
Amplitude of Variation (°F)	±8.75	±10.35	±11.85	±13.85	±13.65	±15.1	±13.2	±9.85	±7.05
Dew Point (°F)	12.1	17.4	17.3	30.4	36.0	39.5	36.9	31.1	27.5
Degree Days	965	679	569	292	128	50	293	633	865
Time of Peak Temperature (PST)	1330								
Average Wind Speed at 7-ft Elevation During Daylight Hours (mph)	4.0	4.5	6.0	7.0	6.0	5.5	4.5	4.0	3.5
h_{fo} ** (mW/cm^{2}K)	1.10	1.17	1.34	1.46	1.34	1.30	1.17	1.10	1.03
h_{fr} (mW/cm^{2}K)	0.31								
h_{ir} † (mW/cm^{2}K)	0.15								
h_{avg} †† (mW/cm^{2}K)	0.85	0.89	0.97	1.03	0.97	0.95	0.89	0.85	0.82

*Climatological data from *Climatology of the Hanford Area*, Report BNWL-1605, UC-53, AEC Contract AT(45-1)-1830

**For air blowing across a 6-inch fin at a 45° angle to vertical.

†h_{ir} evaluated at $\Delta T = 10°C$ and fin width = fin gap = height from roof. $\epsilon_{ir} = 0.85$.

††$h_{avg} = \frac{1}{2}(h_{fo} + h_{fr}) + h_{ir}$.

Table 5

INSOLATION IN RICHLAND (W/m^2) FOR SOUTH-TILTED SURFACES*

Time* (PST)	Jan		Feb		Mar		Apr		May		Sep		Oct		Nov		Dec	
	0°	45°	0°	45°	0°	45°	0°	45°	0°	45°	0°	45°	0°	45°	0°	45°	0°	45°
0430									12.8	5.21								
0530							27.9	17.4	19.8	40.2	8.1	9.4						
0630			1.2	5.05	37.6	613	138	86.2	243	98.9	95.4	111	24.4	67.1	1.2	4.4		
0730	4.7	20.2	35	147	144	235	295	297	407	309	246.6	329	126	346.5	337	124	4.7	25.9
0830	55.8	239	129	316	279	434	449	504	556	511	405	556	258	531	114	418.5	48.8	269
0930	136	398	230	485	410	627	574	680	674	677	531.5	738	367	687	198	534	112.8	374
1030	207	530	323	640	507	769	659	801	746.5	783	621	867.5	445	800	256	614	168.6	472
1130	249	605	377	728	566	856	683	839	781	834	651	911	479	846	279	641	201	528
1230	255	620	385	743	560	847	671	824	741	791	647	906	463	818	267	613	201	528
1330	219	561	349	691	510	774	605	735	694	728	585	817	393	706	220	528	168.6	472
1430	158	463	280	591	429	656	524	620	614	616	476	661	290	543	151	407	107	355
1530	79.1	339	181	443	307	478	396.5	445	490	450	342	470	172	354	65	239	39.5	217.6
1640	15.1	64.8	70	295	170	277	257	259	342	260	191	255	58	160	7	25.7	1.2	6.6
1730			7	29.5	50	81.5	121	75.6	201	81.8	59.3	68.7	4.7	12.9				
1830					1.2	2.0	25.6	16.0	72.1	29.3	4.7	5.4						
1930									8.1	3.3								

*Climatological data from *Climatology of the Hanford Area*, Report BNWL-1605, UC-53, AEC Contract AT (45-1)-1830.

**Hour average centered at this time.

CONVECTION

Under windy conditions, the collector behaves like a flat plate in forced flow; under stagnant conditions, free convection is dominant. Under stagnant conditions and with moderate collector-ambient temperature differences, the thermosyphon flow is laminar and the heat transfer coefficient is given by

$$h_{fr} = \frac{0.29K_a}{L}\left(Gr_{2L}\cos\gamma\right)^{1/4} \qquad (W/cm^2k) \qquad 3\text{-}18$$

where:

K_a = thermal conductivity of air,

Gr_{2L} = Grashof number based on the length (2L), and

γ = angle the plate makes with vertical.

As the angle γ increases toward 90°, the preceding equation breaks down and free convection from a horizontal plate must be considered.

In the event of wind, the heat transfer coefficient is typical of that for a tilted plate in forced flow; however, most experiments have been performed with untilted plates[5] and the average heat transfer coefficient for a wind perpendicular to the panel axis is estimated to be

$$h_{Fo} = \frac{0.295K_a}{L}\left[Re_{2L}\cos\left(\frac{\pi}{2} - \gamma\right)\right]^{1/2} \qquad (W/cm^2k) \qquad 3\text{-}19$$

where Re_{2L} is the plate Reynolds number based on (2L), and the factor $\cos(\pi/2 - \gamma)$ accounts for the velocity component parallel to the collector surface. This equation is not valid for heat transfer from the rear of the fin, but in analogy to results for separated flow from spheres and cylinders, the heat transfer coefficient can be expected to be of similar magnitude.[6] Table 4 includes the anticipated convective heat transfer coefficients h_{Fo} and h_{Fr}.

INFRARED RADIATION

The radiative transfer at far infrared (IR) wavelengths is similar to that in the solar spectrum with several complications: the ambient source/sink is diffuse rather than localized, and the absorbed solar on the rear reflective surface creates a regular array of stripe pattern heat sources on that surface. In addition, the IR radiative sink temperature of sky and cloud cover during daylight hours is not well documented. Generally, it is assumed that diffuse solar radiation input overwhelms any IR radiation loss to the sky. For this collector, IR radiative heat transfer does not appear to be a dominant mode of energy transport and has been modeled as a heat transfer coefficient using the relatively crude approach

$$h_{ir} = \left[\frac{\sigma\varepsilon_{ir}\left(T_a^{\,4} - T_o^{\,4}\right)}{2\left(T_a - T_o\right)}\right]\left[\left(1 - F_{cs}\right)\left(1 + F_t\right)\right] \qquad 3\text{-}20$$

where:

σ = Stefan-Boltzman constant, and

ε_{ir} = hemispherical total emissivity of the collector at collector tube temperature T_o.

The view factor of the collector-sky combination is F_{cs}, and it is assumed there is not net transfer of heat at far IR wavelengths with the daytime sky. Table 4 includes the expected values of h_{ir}.

RAINFALL

The heat input to a direct-expansion solar collecting heat pump resulting from rainfall on the collector surfaces has been calculated for an example case and found to be an insignificant source of heat. Details are provided below. In addition, the rainfall causes mixing in the convection boundary layer, which considerably improves condensation and convective heat transfer. No suitable way to model this effect has been found.

Observations indicate that, except at very high rainfall rates ($\geq$ 1 cm/hr) or steep collector tilts (θ >70°), the water contributed by an individual raindrop remains on the fin surface long enough for it to reach essentially the same temperature as the fin. By using this observation and assuming a uniform fin temperature, the heat input to the solar-assisted heat pump can be calculated. Assuming the rain is falling vertically, the mass flux of water hitting the fins surface is given by:

$$m''\left(\frac{Kg}{m^2 - hr}\right) = \left(\dot{h}\frac{cm}{hr}\right)\left(\frac{10\ Kg\ H_2O}{cm\ m^2\ H_2O}\right)\cos(\theta) \qquad 3\text{-}21$$

where:

m'' = mass flux of water [$Kg/(m^2 - hr)$],

$\dot{h}$ = rainfall rate (cm/hr), and

θ = collector tilt from horizontal.

The heat input into the fin is

$$Q''_{RF} = m''\ Cp\left(T_R - T_F\right) \qquad 3\text{-}22$$

where:

Q''_{RF} = heat input due to rainfall (W/m^2),

Cp = heat capacity of water [$(W - hr)/(Kg - °C)$],

= 1.166[$(W - hr)/(Kg - °C)$] @ 10°C,

T_R = rain temperature (°C), and

T_F = average fin temperature (°C).

An example calculation shows that rainfall is not a very significant direct source of heat for the solar-assisted heat pump.

$\dot{h} = 0.254$ (cm/hr) = 0.1 (in./hr)

$\theta = 60°$

$T_R = 15°C = 59°F$

$T_F = 1°C = 34°F$

$m'' = (0.254)(10) \cos(60) = 1.493$ [Kg/(m^2 - hr)]

$Q''_{RF} = (1.493)(1.166)(15 - 1) = 24.4$ (W/m^2) .

The action of rainfall in improving convective heat transfer between the air and the fins is not amenable to analysis. It is known that convective heating transfer is improved considerably due to mixing in the boundary layer caused by the rainfall.

Experimental data from the operation of the solar-assisted heat pump may lead to an empirical relationship for this indirect effect of rain on convective heat transfer.

CONDENSATION

Condensation provides heat input to the solar-assisted heat pump due to the large heat of condensation of water vapor. An exact calculation of the heat input due to condensation is difficult in that knowledge of the velocity field surrounding the collector fins is necessary. It is difficult to define these fields in general due to their dependence on natural convection, wind speed, wind direction, etc.; however, an estimate can be made in the following manner.

The molar flux of water to the fin surface is given by Bird, Stewart, and Lightfoot[7] as:

$$N = \frac{cD}{\delta} \ln\left(\frac{1 - X_o}{1 - X_\delta}\right) \qquad 3\text{-}23$$

where:

N = molar flux of water [g-mol/(cm^2 - s)],

c = molar density of air and water (g-mol/cm^3),

D = diffusivity of water vapor in air (cm^2/s),

X_o = mole fraction of water vapor in air at the fin surface,

X_δ = mole fraction of water vapor in air outside of the boundary layer, and

δ = boundary layer thickness for diffusion (cm).

The diffusivity, D, of water vapor in air is given by Bennett and Myers[8] as being 0.256 cm^2/s at 25°C. Bird, et al.,[7] show that

$$D(T) = D\left(T_{ref}\right)\left(\frac{T}{T_{ref}}\right)^{3/2} \qquad 3\text{-}24$$

where:

T = temperature (K),

T_{ref} = reference temperature (K), and

$D\left(T_{ref}\right)$ = reference diffusivity (cm^2/s).

Thus, at a film temperature of 5°C,

$$D = 0.256\left(\frac{278.16}{298.16}\right)^{3/2}\left(\frac{cm^2}{s}\right) = 0.231\ \frac{cm^2}{s}$$

Using the ideal gas law, the molar density of the atmosphere is

$$c = \frac{P}{RT} \quad .$$

For:

$P = 1$ atm,

$T = 5°C = 278.16$ K, and

$R = 82.05$ $(cm^3$ atm$)/($g-mol K) this factor is then

$c = [1/(82.05)(278.16)] = 4.38[10^{-5}(\text{g-mol}/cm^3)]$.

The mole fraction of water vapor, x, can be calculated for saturated vapor from knowledge of vapor pressure versus temperature.

$$X(T) = \frac{P_{vap}(T)}{1 \text{ atm}} \quad .$$

Over a limited temperature span, the vapor pressure versus temperature relationship is given by the Clapeyron equation.[9]

$$\ln P_{vap} = A - \frac{B}{T} \quad . \qquad 3\text{-}25$$

For the temperature range of -10°C to 30°C and for the vapor pressure expressed in mm-Hg, the appropriate values of A and B are 21.7542 and -5538.96, respectively, where T is in degrees Kelvin. Thus, X(T) is given by

$$X(T) = \frac{\exp\left[21.7542 - \left(\frac{5538.96}{T}\right)\right]\left[\text{mm-Hg}\right]}{760\left(\frac{\text{mm-Hg}}{\text{atm}}\right)} \quad , \text{ or}$$

$$\ln(X) = 21.7542 - \left(\frac{5538.96}{TK}\right) - \ln(760)$$

$$\ln(X) = 15.1209 - \left(\frac{5538.96}{TK}\right)$$

$$X(T) = \exp\left[15.1209 - \left(\frac{5538.96}{TK}\right)\right] .$$

Thus:

$$X_o = X\left(T_F\ K\right) \quad , \text{ and}$$

$$X_\delta = X\left(T_{DP}\ K\right)$$

where:

T_F = average fin temperature (K), and

T_{DP} = dew point (K).

The boundary layer thickness, δ, for laminar flow is given by Levich.[10]

$$\delta_\ell = 3\left(\frac{D}{\nu}\right)^{1/3}\left(\frac{\nu\ell}{u}\right)^{1/2} \qquad 3\text{-}26$$

where:

D = diffusivity of water vapor through air (cm^2/s),

u = air velocity far from the fin (cm/s),

ν = kinematic viscosity (cm^2/s),

ℓ = position from leading edge of fin (cm), and

δ_ℓ = boundary layer thickness at position L.

The average boundary layer thickness δ is given by

$$\delta = \frac{\int_o^L \delta_\ell d\ell}{L}$$

where L equals the total fin width. Evaluating the integral yields

$$\delta = 2\left(\frac{D}{\nu}\right)^{1/3}\left(\frac{\nu L}{u}\right)^{1/2} \quad . \qquad 3\text{-}27$$

The kinematic viscosity of air, ν, at 5°C is $1.47(10^{-4}$ $ft^2/s)$ or 0.137 cm^2/s.

Thus:

$$\delta(\text{cm}) = 2\left[\frac{0.231}{0.137}\right]^{1/3}\left[0.137\right]^{1/2}\left[\frac{L(\text{cm})}{u\ \frac{\text{cm}}{\text{s}}}\right]^{1/2} = 0.881\left[\frac{L(\text{cm})}{u\ \frac{\text{cm}}{\text{s}}}\right]^{1/2} \quad , \qquad 3\text{-}28$$

and the expression for the molar flux of water becomes

$$N\left(\frac{\text{g-mol}}{\text{cm}^2 - \text{s}}\right) = \frac{[4.38\ (10^{-5})]\,[0.231]}{0.881\left[\frac{L(\text{cm})}{u\left(\frac{\text{cm}}{\text{s}}\right)}\right]^{1/2}}\ \ln\ \frac{1 - \exp\left[15.1209 - \left(\frac{5538.96}{T_F\ \text{K}}\right)\right]}{1 - \exp\left[15.1209 - \left(\frac{5538.96}{T_{DP}\ \text{K}}\right)\right]}$$

$$= \frac{1.15\ (10^{-5})}{\left[\frac{L(\text{cm})}{u\left(\frac{\text{cm}}{\text{s}}\right)}\right]^{1/2}}\ \ln\ \frac{1 - \exp\left[15.1209 - \left(\frac{5538.96}{T_F\ \text{K}}\right)\right]}{1 - \exp\left[15.1209 - \left(\frac{5538.96}{T_{DP}\ \text{K}}\right)\right]} \quad . \qquad 3\text{-}29$$

The heat input due to condensation is given by

$$Q''_{cond}\left(\frac{W}{m^2}\right) = Nh_{fg}\left(10^4\frac{cm^2}{m^2}\right) \qquad 3\text{-}30$$

where h_{fg} is the heat of vaporization of water in watts per second per gram-mole,

$$h_{fg} = 4.49\ (10^4)(\text{W-s/g-mol}) \quad ,$$

and the resulting expression for heat input due to condensation is

$$Q''_{cond}\left(\frac{W}{m^2}\right) = \frac{5160}{\left[\frac{L(\text{cm})}{u\left(\frac{\text{cm}}{\text{s}}\right)}\right]^{1/2}}\ \ln\ \frac{1 - \exp\left[15.1209 - \left(\frac{5538.96}{T_F\ \text{K}}\right)\right]}{1 - \exp\left[15.1209 - \left(\frac{5538.96}{T_{DP}\ \text{K}}\right)\right]} \quad . \qquad 3\text{-}31$$

Example calculations:

$L = 15.24 \text{ cm} = 6 \text{ in.}$

$u = 223.5 \text{ cm/s} = 5 \text{ mi/hr}$

$T_F = 274.2 \text{ K} = 1°C$

$T_{DP} = 281.2 = 8°C$

$$Q''_{cond}\left(\frac{W}{m^2}\right) = \frac{5160}{\left(\frac{15.24}{223.5}\right)^{1/2}} \ln \frac{1 - \exp\left[15.1209 - \left(\frac{5538.96}{274.2}\right)\right]}{1 - \exp\left[15.1209 - \left(\frac{5538.96}{281.2}\right)\right]}$$

$$= 1.98(10^4) \ln\left(\frac{0.9938}{0.9897}\right) = 81.2 \text{ W/m}^2.$$

Note: This is the value for one side of the fin only. The actual value would be twice this value or 162 W/m^2.

Hence, condensation heat transfer can account for 15-25% of heat transfer near solar noon and a larger fractional amount under overcast conditions or during sunrise/sunset times of day. In areas with high humidity and moderate winds, the heat input due to condensation would, of course, become more significant and may be comparable to solar input rates.

Example calculations:

$L = 15.24 \text{ cm} = 6 \text{ in.}$

$u = 670.5 \text{ cm/s} = 15 \text{ mi/hr}$

$T_F = 274.2 \text{ K} = 1°C$

$T_{DP} = 293.2 \text{ K} = 20°C$

$Q'' = 3.42(10^4) \ln\left(\frac{0.9938}{0.9770}\right) = 584 \text{ W/m}^2$ (one side) $= 1{,}168 \text{ W/m}^2$ (both sides).

This is a water condensation rate of 0.844 (Kg H_2O/m^2-hr-side) or 0.8 mm/hr.

COLLECTOR STRUCTURAL ANALYSIS

As in the case of conventional flat plate collectors, consideration of external loading due to winds or snow and ice accumulation is necessary to insure the structural integrity of the present design. Of these three external loads, the most severe arises from wind forces since a 60-mph wind striking a plate perpendicular to the air stream exerts as much force as an accumulation of 3.6 inches of ice or 16.4 inches of snow (ρ_{snow} = 12.5 lb/ft^3) does on a horizontal member. In addition, use of a hot-gas bypass system or reversal of the heat pump operation can dispose of snow or ice layers. It should be noted that both these systems are commonly used to rid conventional air-to-refrigerant evaporators of excess condensate buildup.

The primary goal of the structural support analysis was to determine the permissable spacings for collector-to-roof attachment brackets. To obtain this information, the wind loading was assumed to be that of an air stream striking a flat plate perpendicular to the air stream direction, with the plate's projected area being that used in the force calculations. All structural members were assumed to be initially straight, and maximum wind speed was set at 60 mph.

With these assumptions and values, calculations were carried out for various combinations of fin and tube sizes as well as various types of fin stiffeners. The results for three such designs are shown in Figure 11, with the maximum fin or tube stress being shown as a function of attachment bracket spacing. Since the fin sections at each end of each horizontal row are subjected to a bending moment at one support and essentially are simply supported at the other (ends of row), bending stresses are higher than in the interior sections of the fin and tube wherein bending moments are encountered at both supports. For this reason, two horizontal dashed lines are used in the figure: the lower refers to the end fin sections, and the upper to the center fin sections. Of the two lines, the lower intersects

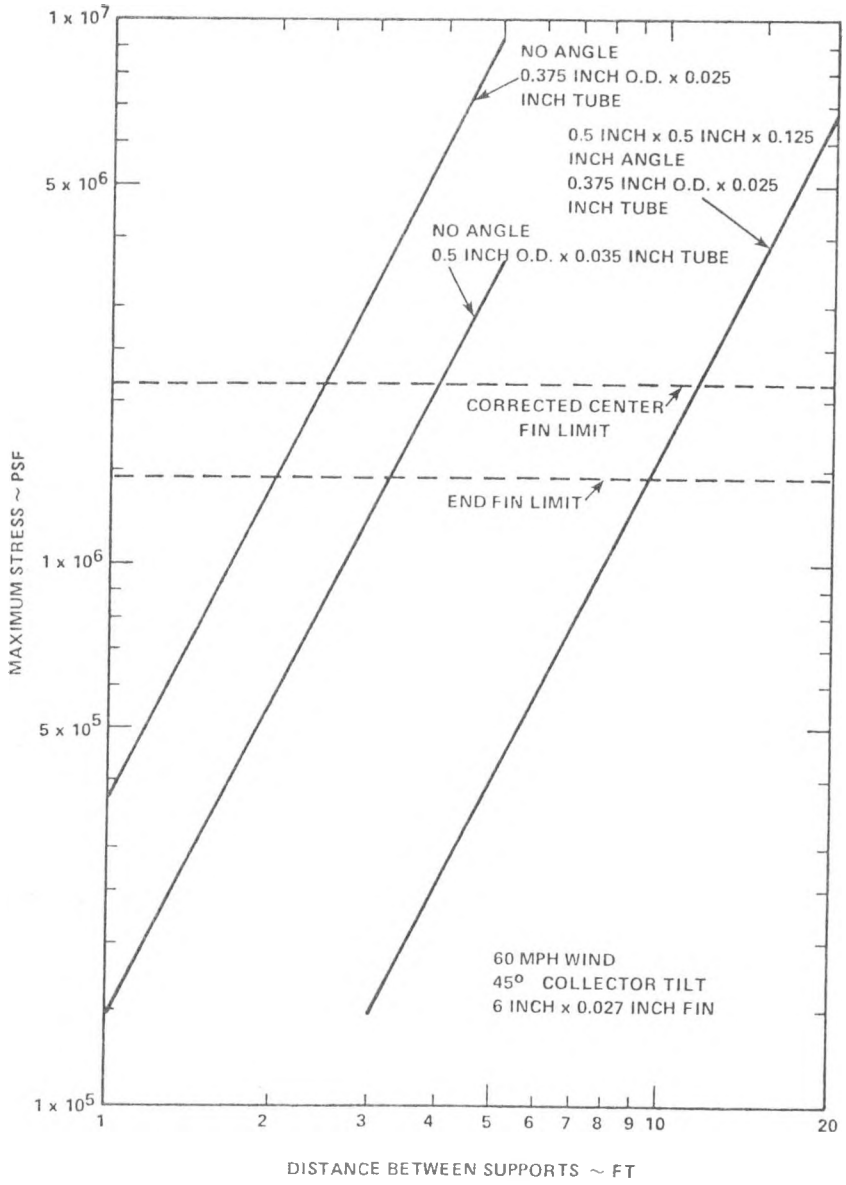

Figure 11. Bending Stress Results for the Determination of Support Spacing.

the ordinate at the true yield stress, while the upper represents a pseudo-yield stress that accounts for the lower bending stress level in the central portions of a fin row. The maximum premissible bracket spacing is determined from the intersection of these lines with the bending stress levels.

For the fin and tube above, bracket spacings of 3 ft and 3.5 ft are indicated for the 0.375-in. OD tube and 4.2 ft and 4.7 ft for the 0.5-in. This increase of 6-8 ft in the permissible spacing is significant in that it decreases the number of brackets required and reduces the amount of time needed for installation. Where the homeowner elects to employ professionals to carry out the installation, this saving can be significant.

To inhibit corrosion between the copper and steel, thin synthetic standoff clips (Figure 5) are used between the tube and angle as well as insulating spacers between the fin and bracket. Thus, the two dissimilar metals are electrically insulated and the possibility of a galvanic cell forming is precluded. In addition, paint cannot be rubbed from the angle's surface and rust formation is inhibited.

Section 4

SYSTEM CONTROLS AND MONITORING

The control system of a solar-assisted heat pump must, for normal service, operate in the conventional mode with heat being supplied on demand according to the temperature in the conditioned space. Conventional controls can be adapted for this requirement.

It is probable that the system efficiency (COP) can be improved by varying the volume capacity of the compressor to match the load requirements. A variable-frequency motor drive circuit is incorporated in the system to provide this capability.

The state of the system is monitored by measuring temperature at various points. Control of frost buildup on solar collector/evaporator surfaces is to be accomplished with a hot-gas bypass system. It is expected that temperatures and motor conditions will signal the need to remove frost. Replacement of the conventional expansion valve with a commanded valve has possible advantages. A microcomputer handles overall control and monitoring tasks. Figure 12 is a schematic of the heat pump system, showing control and monitoring points.

SPEED CONTROL

Control of the compressor capacity on Sigma's demonstration unit is managed by varying the speed of the drive motor. A commercially available ac motor control, Parajust 7010 (from Parametrics, Orange, Connecticut), rectifies 230-V, single-phase input power to dc; then, it generates a three-phase ac output using switching transistors. An analog input voltage controls the output frequency as required. Output voltage is controlled in proportion to frequency to protect the motor from overheating. An overload trip is incorporated into this circuit to protect against excessive motor current.

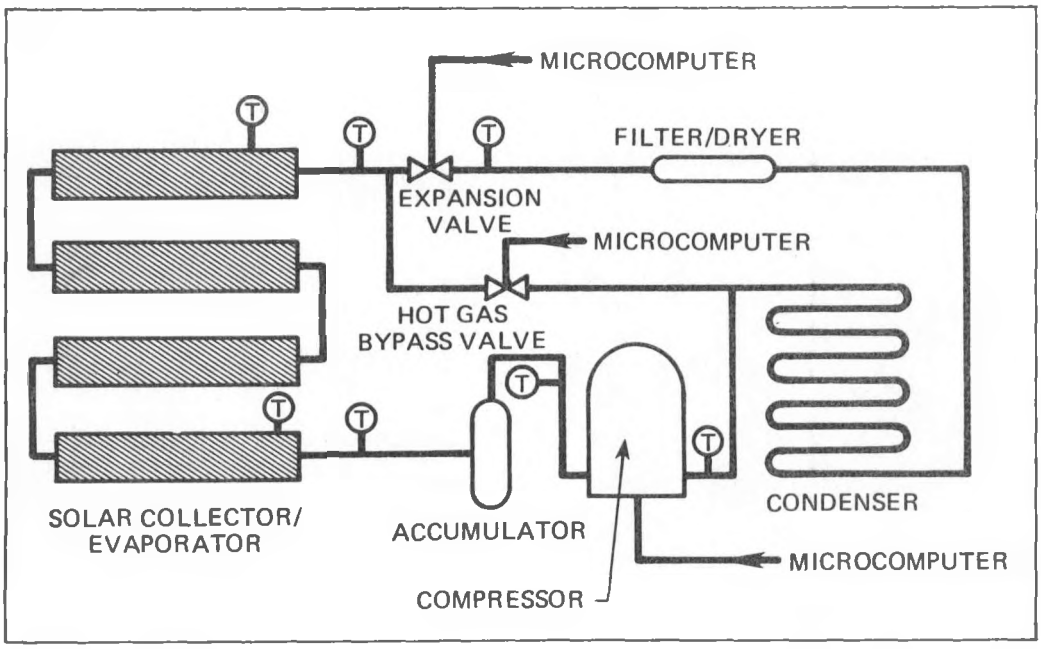

Figure 12. Solar Heat Pump Schematic Showing Themocouple Locations. Expansion Valve was Thermostatically Controlled for These Tests.

The command circuitry of the motor speed controller is referenced to the hot side of the 230-V input line. An isolating interface is required between the microcomputer and the speed control. A suitable isolator is available from Parametrics, or one can be built to suit.

MICROCOMPUTER CONTROL SYSTEM

The heart of the control system is a microprocessor, which receives analog temperature signals and sends control signals via an appropriate interface.

In the demonstration unit, the processor is an Apple II™ microcomputer and the interface is an Analog Devices RTI-1225 analog input/ouput module. System control is via the computer keyboard, with system status readout on

the computer terminal. System temperature readings are updated about once per second.

The equipment used for this demonstration system is not the hardware that would be used in a commercial version of the system. The requirements for monitoring and logging conditions in the demonstration unit are managed most suitably with the complete microcomputer system, which would be replaced by a card-based microprocessor in a commercial version. A typical microprocessor is available from Prolog™ at roughly $150 (in quantities of 100).

Section 5

FEATURE TESTS

The Sigma Research, Inc., direct-expansion solar collector (7.4 m^2) was modified to include a variable capacity compressor heat pump system and fitted with an improved heat rejection arrangement. The unit was tested under early summer conditions to verify the analytical efforts of the project. Coefficients of performance fell in the expected range, but difficulties in the electrical power measurements lead to rather large uncertainties in the results. More thorough testing would be desirable.

HARDWARE CONFIGURATION

The Sigma prototype shown in Figure 7 was fitted with a variable capacity compressor system using a two-cylinder open-frame compressor (Victaulic 16436) with 1.438-in. bore and 1.375-in. stroke. Motive power was supplied by a 230-V, three-phase motor of 1.5 horsepower nameplate rating. The motor speed control described in Section 4 drove this motor at a variable speed by synthesizing the appropriate power frequency under control of the microcomputer.

A standard thermostatic expansion valve with external equalizer (Danford TEX 2) was fitted to the system, which was then charged with R-22 refrigerant. Thermocouples were placed at various points around the refrigerant circuit as indicated in Figure 12 and were insulated to isolate the attachment points from ambient conditions.

The necessary hardware for logging temperature measurements via the Apple II™ microcomputer was not available during the testing period, so a Digitrend 220 datalogger was used to produce a paper tape printout of temperatures.

Compressor suction and discharge pressures were measured using standard refrigeration equipment and recorded by hand.

To maintain heat rejection conditions in the temperature range required for heating applications, a closed-loop air circulation duct system was attached to the condenser. Air circulated within this loop by a fan carried heat from the heat pump condenser to a water-cooled heat exchanger. Power consumed by the fan motor was not measured or included in the performance accounting.

ELECTRICAL MEASUREMENTS

During the tests, the ac input voltage to the motor speed control and the current in one of the three-phase legs to the motor were recorded. During data reduction following the test period, it was realized that these measurements did not give the motor input power, since the speed control alters the voltage applied to the motor according to the speed setting. In addition, it was found that the clip-on ammeter used for current measurement gave correct readings only at 60 Hz.

An empirical calibration curve was constructed to relate the readings taken during tests to the actual power demand of the speed control circuitry. Any possible difficulty with a nonunity power factor was avoided by measuring dc voltage and current within the speed control unit. The appropriate calibration factor for each operating frequency was applied to the readings taken during testing to obtain the electrical power draw of the system.

CONDITIONS DURING TESTS

Testing was carried out in early June, and ambient temperatures and solar input were both higher than in a typical heating application. Testing, therefore, was confined to the hours before 1300 standard time ($\simeq$ solar time) to avoid overloading the system. The sky was clear to partly cloudy except for one overcast day. Ambient temperatures ranged from 53°F to 74°F and winds were light to moderate. No frost formed on the collector surfaces.

DATA REDUCTION

The coefficient of performance for a heat pump is the ratio of heat delivered at the condenser to the electrical energy consumed. In terms of the refrigerant enthalpy at the condenser inlet, h_c, and at the condenser outlet, h_o, this becomes

$$COP = \frac{\dot{m}(h_c - h_o)}{P_h} \qquad 6\text{-}1$$

where $\dot{m}$ is the mass flow rate of refrigerant and P_h is the electrical input to the compressor in the same units. If Btu/hr is used for heat flow in the refrigerant circuit, then

$$P_h\left(\frac{Btu}{hr}\right) = 3.413\ P_e(W), \qquad 6\text{-}2$$

given the electrical power P_e.

The mass flow rate, $\dot{m}$(lb/hr), is given by

$$\dot{m} = \frac{60V}{v}, \qquad 6\text{-}3$$

where v is the specific volume of the refrigerant (ft^3/lb) at compressor inlet conditions, and V is the compressor volumetric flow rate (ft^3/min). This factor is the product of compressor displacement and its volumetric efficiency E. In terms of compressor parameters, this becomes

$$V = \frac{\left(\frac{\pi}{4}\right)D^2LNCE}{1728} \qquad 6\text{-}4$$

where:

D = cylinder diameter (1.438 in.),

L = stroke (1.375 in.),

C = number of cylinders (2),

N = compressor speed (rpm), and

$$E = 1.058 - 0.06746 \left(P_D/P_S\right) \qquad 6\text{-}5$$

with P_D and P_S being compressor discharge and suction pressure (psia).[11]

Collecting Eq. 6-3 through 6-5 gives

$$\dot{m} = \left(0.1640 - 0.01048 \frac{P_D}{P_S}\right)\left(\frac{N}{v}\right) \qquad 6\text{-}6$$

for the mass flow rate.

Data reduction, therefore, involves obtaining v from the compressor suction pressure and temperature using tables or an equation of state expression, and combining this result with the rotational speed and compressor pressure ratio using Eq. 6-6 to obtain the mass flow rate $\dot{m}$. Enthalpys at the condensor inlet and outlet are obtained, again using tables or some equation of state expression, from knowledge of the pressures and temperatures at these points. Eq. 6-1 then gives the coefficient of performance.

For this test series, data were reduced by hand using ASRE tables.[12] The pressure drop across the condenser was neglected; both h_c and h_o were evaluated at the compressor discharge pressure.

RESULTS AND DISCUSSION

Variations during the course of one day's testing in some of the external parameters of the solar heat pump system are shown in Figure 13. Note the jump in coefficient of performance when the compressor speed was reduced. The insolation values are hourly averages as observed at the Hanford Meteorological Station. Some of the lack of correlation between periods of maximum

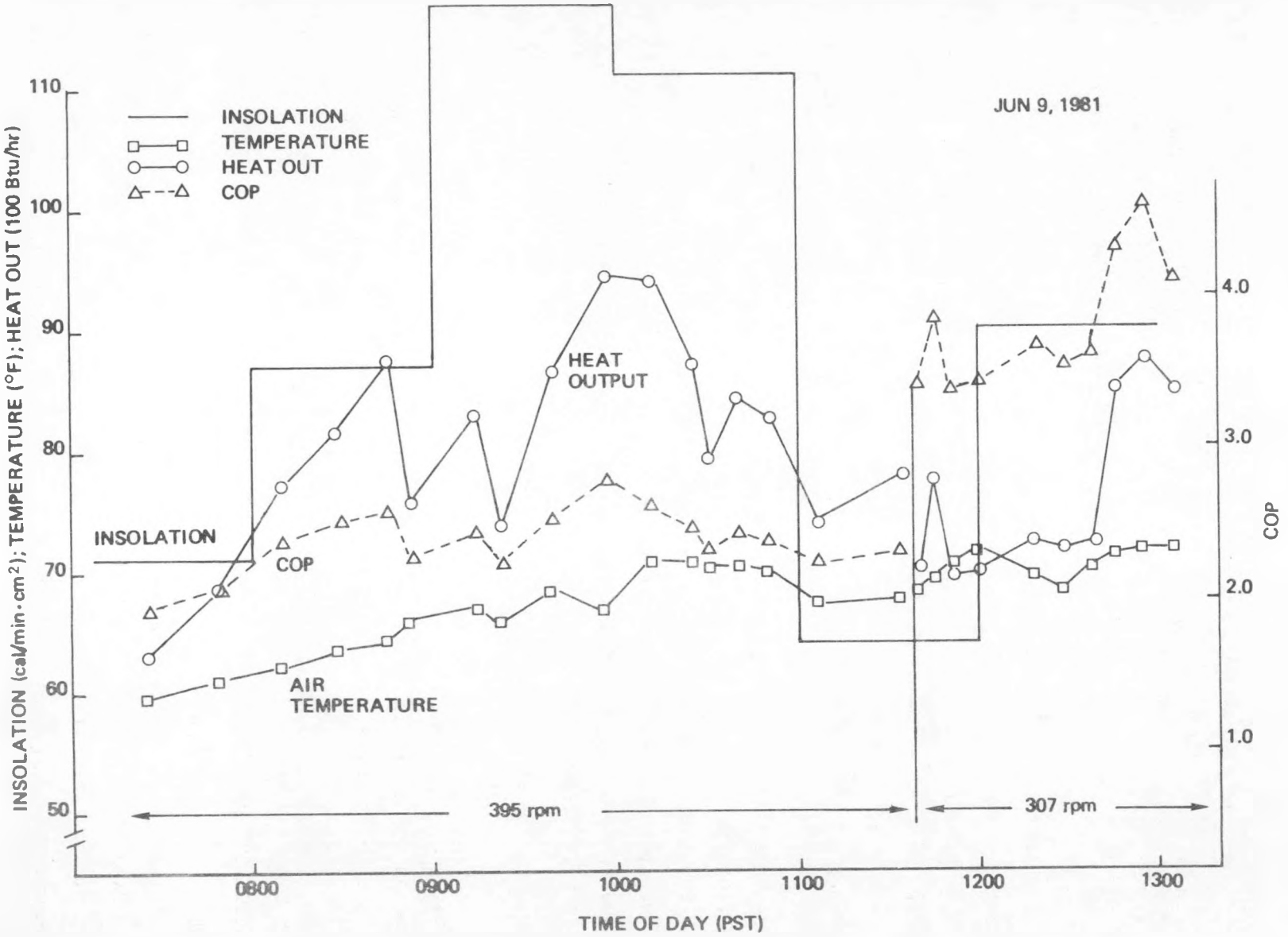

Figure 13. External Parameters for Test 0609.

output and periods of maximum insolation is likely due to the 25-mile separation between the Sigma facility and the measuring station.

Figure 14 shows the corresponding variation in refrigerant pressures and temperatures at a few points in the system. There is evidence that the change of speed at 1135 introduced a transient into the system that took about 20 minutes to disappear. Also, during some periods the solar input was large enough to drive the compressor suction temperature above ambient temperature, though during most of the day it remained a few degrees below ambient. The large COP values observed around 1300 (Figure 13) are associated primarily with increased suction pressure.

Figure 15 summarizes coefficient of performance results for the whole test series as a function of the heat flow to the condenser. Significant dependence on the compressor's rotational speed is seen, with the slowest speed (307 rpm) showing the highest COP at a given heat output. Clearly, the work needs to be extended to an even lower rpm, and a larger range of heat throughputs must be investigated. Ambient temperatures and solar inputs were both higher in these tests than would be typical of a heating season; this tends to make the COP higher than typical.

DIRECTIONS FOR FURTHER WORK

Two lines of effort deserve additional work: collecting a complete set of data on the operating characteristics of the prototype direct-expansion solar collector system, and working out a collector design that is commercially practical.

Operating Characteristics of Prototype Collector

The heat pump system in the present direct-expansion solar collector has not had a complete test. An extensive series of tests should be conducted in fall, winter, and spring weather over a range of solar inputs and ambient temperatures. This will require more complete automation of the data collection arrangement, including the reading of system pressures, and electrical

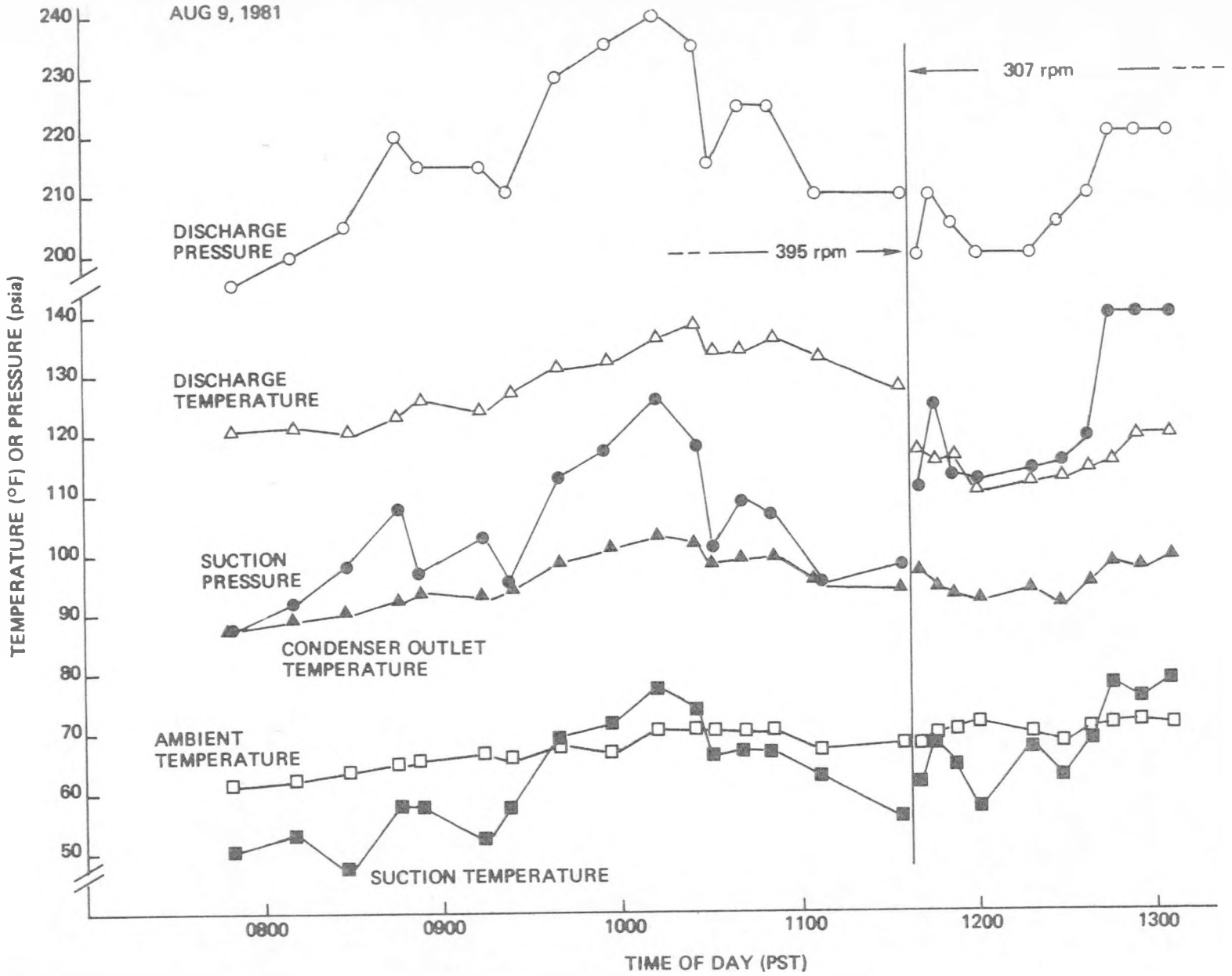

Figure 14. Heat Pump Conditions for Test 0609.

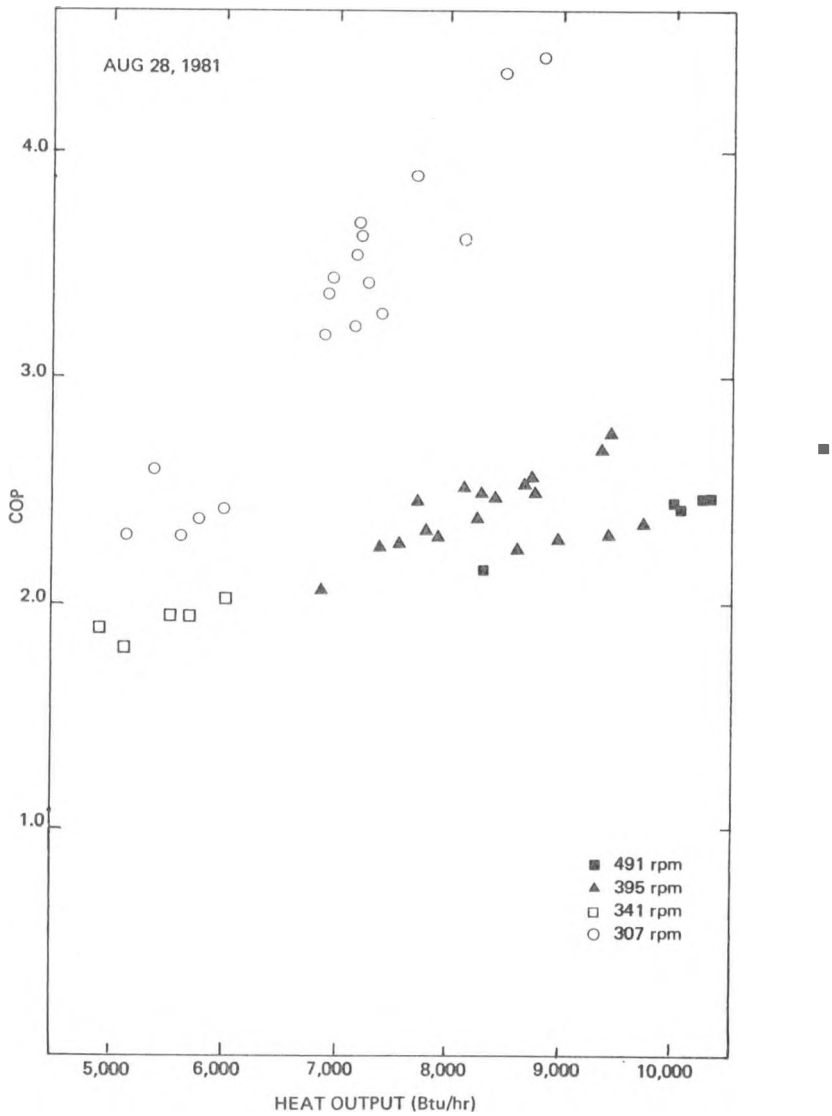

Figure 15. COP Versus Heat Output Over Whole Test Series.

power demand. Additional work is necessary to make the data reduction procedure correspond to the methodology of the heat pump modeling. Real-time comparisons of expected and achieved performance ought to be attempted.

Commercial Collector Design

The outstanding feature of the direct-expansion solar collector concept is that there is no necessity for glazing or insulation since the collector surfaces operate near or below ambient temperature. The collector system can, therefore, be much cheaper than the usual flat-plate collector. Additional savings are possible if the collector surfaces can substitute for shingles or siding on the south-facing portion of buildings. Effort should be directed toward the design of a collector that can be mass-produced cheaply and can serve as the exterior surface of a house while, at the same time, providing an input of solar heat to the heat pump system.

Section 6

SYSTEM ANALYSIS AND OPTIMIZATION

HEAT PUMP MODELING

A numerical model of a nonideal heat pump was generated for use in system analysis and optimization. The model incorporates superheat and subcooling corrections as well as valve frictional pressure drops and nonideal gas effects.

Thermodynamic Cycle

The model is based on the pressure-enthalpy diagram shown in Figure 16, which is described below.

- Point 0 — Condensate at an intermediate point within the heat rejection heat exchanger where the vapor-liquid quality is exactly zero.
- Point 1 — Subcooled liquid at the entrance to the expansion valve.
- Line Segment (Point 1 - Point 2)

  Irreversible constant enthalpy expansion of saturated liquid from pressure P_1 to P_2.
- Line Segment (Point 2 - Point 3)

  Reversible addition of heat at constant pressure in the heat input heat exchanger.
- Line Segment (Point 3 - Point 4)

  Superheating of working fluid vapor caused by heat transfer from input heat exchanger, suction line, and compressor case.
- Line Segment (Point 5 - Point 6)

  Additional heat transfer within compressor cylinder. (Pressure drops within the suction line and inlet valves represented by pressure difference P_5 minus P_4.)

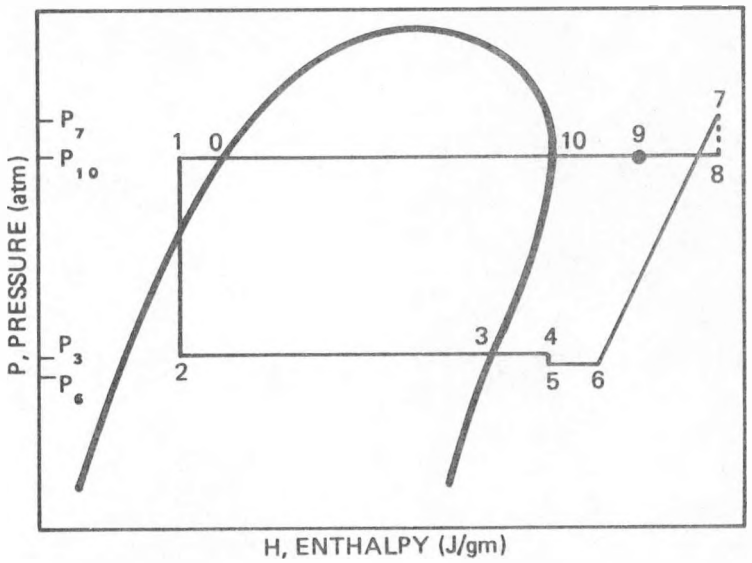

Figure 16. Pressure-Enthalpy Diagram for Solar Heat Pump Thermodynamic Cycle.

- Line Segment (Point 6 - Point 7)

  Reversible and adiabatic compression of superheated vapor within compressor from inlet pressure $P_{5/6}$ to discharge pressure P_7. (The discharge pressure of P_7 is somewhat higher than the condenser saturation pressure P_{10} because of the frictional losses in the compressor discharge valves and line.)

- Line Segment (Point 8 - Point 9 - Point 0 - Point 1)

  Heat loss from the compressor discharge line, heat rejection heat exchanger, and condensate line up to expansion valve.

Work Input

An approach discussed by Threlkeld[13] was used to calculate the actual pressure-volume (PV) work required to transport a unit mass of working fluid through the thermodynamic cycle, and the PV diagram shown in Figure 17 was the basis for computations of mass transfer and work input to the compressor. A polytropic process was assumed; i.e., gas was assumed to follow the path equation $PV^n = C$ where V is the instantaneous cylinder volume and n is a number unique to each working fluid gas and particular process.

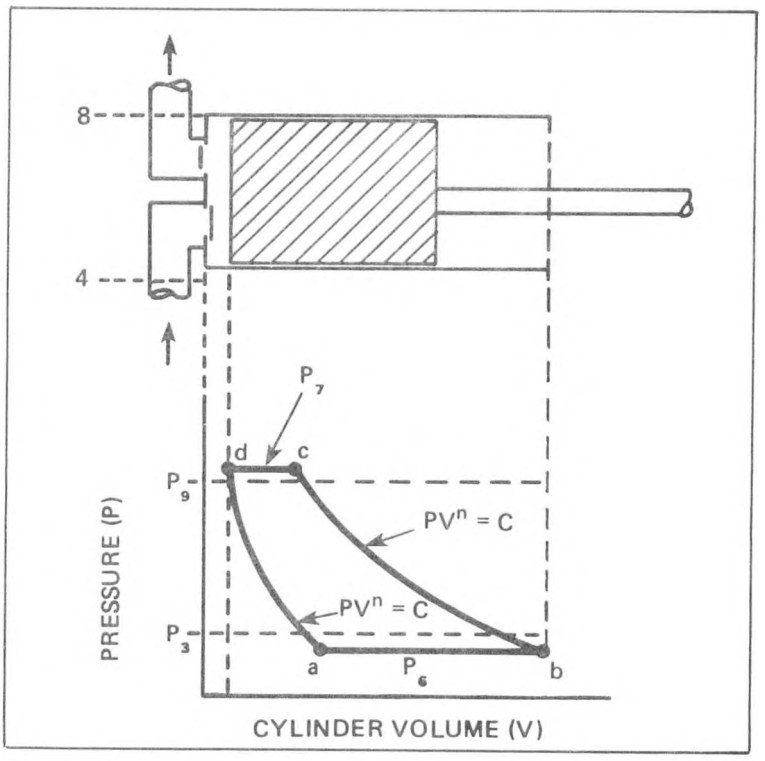

Figure 17. PV Model for Solar Heat Pump Compressor.

Cold gas flows into the cylinder on the intake stroke at pressure $P_{5/6}$, which is less than saturation pressure P_3 because of intake valve pressure drop. Relatively high temperatures of the compressor can and cylinder wall heat the gas on the intake stroke, and its density is reduced to that at Point 6 in relation to the density of the gas at Point 5 (see Figure 16). Compression from Point b to Point c (Figure 17) raises the vapor to the discharge pressure P_7. The compression process is assumed to be polytropic, so that the path equation has the form

$$PV^n = C \qquad 7\text{-}1$$

where n is a number unique to each working fluid and particular process. The compressed vapor is released at constant pressure to the discharge line, which is at the high-side saturation pressure P_9. Vapor remaining in the cylinder clearance volume expands from condition d to condition a (see Figure 17).

Assuming that the gas does not change in temperature during the process segments a/b and c/d (Figure 17), and that the exponent n is a constant for the compression and expansion processes, the volumetric efficiency can be found to be given by

$$n_v = \left[1 + C - C\left(\frac{P_7}{P_6}\right)^{(1/n)}\right]\left[\frac{\rho_6}{\rho_4}\right] \qquad 7\text{-}2$$

where:

$$C = \frac{\text{piston top-end clearance volume}}{\text{piston displacement volume}} = \frac{V_c}{V_d} \qquad 7\text{-}3$$

and where ρ_4 and ρ_6 refer to the gas densities at Points 4 and 6 in Figure 16. The rate of mass flow through the compressor is

$$\dot{m} = \left[1 + C - C\left(\frac{P_7}{P_6}\right)^{(1/n)}\right]\left[\rho_6 V_d f\right] \qquad 7\text{-}4$$

where f is the rotational rate of the crankshaft.

Power input to the compressor is equal to

$$Q_e = f\left(\int_b^c V dp - \int_e^d V dp\right) \quad . \qquad 7\text{-}5$$

Using the polytropic process Eq. 7-1, the power input to the compressor for PV work is

$$Q_e = \left[\frac{n}{n-1}\right]\frac{P_6}{\rho_6}\left[\left(\frac{P_7}{P_6}\right)^{(n-1)/n} - 1\right]\dot{m} \quad . \qquad 7\text{-}6$$

At this point in the modeling, pressure drops in the suction and discharge lines and in the heat exchangers are neglected.

Fluid Properties

The enthalpys of the liquid and saturated working fluid vapor are given by empirical curve-fit polynominals of the form

$$H_{\ell,sv} = A_1 + B_1T + C_1T^2 + D_1T^3 + \ldots. \qquad 7\text{-}7$$

where A_1, B_1, C_1, D_1, ... are least-squares coefficients fitting experimental data, and T is the absolute temperature in Kelvin degrees. Enthalpy changes at constant pressure for superheated vapor are calculated using the saturated vapor heat capacity C_{ps},

$$\Delta H_{sh} = \int_{T_1}^{T_2} C_{ps}dT = \left(B_2T + C_2T^2 + D_2T^3 + \ldots\right)_{T_1}^{T_2} \quad (J/gm) \qquad 7\text{-}8$$

where once again the coefficients are obtained by least-square fitting of experimental data. Saturation vapor pressure is computed using a curve-fit equation of the form

$$P_s = \frac{P_o}{T^m} \exp\left(\frac{A}{T}\right) \qquad 7\text{-}9$$

where P_o, M, and A are constants obtained through curve-fitting of data.

Working fluid gas densities are calculated iteratively using the Hirschfelder, Buehler, McGee, and Sutton equation of state.[14] The gas compressibility factor, z, is given by

$$z = \left(\frac{M}{T_r} + \frac{N}{T_r^2}\right)\rho_r + P\left(1 - \frac{1}{T_r^2}\right)\rho_r^2 + \left(\frac{1}{1 + RP_r + SP_r^2}\right) \qquad 7\text{-}10$$

where:

$$T_r = T/T_c,$$

$$\rho_r = \rho_g/\rho_c,$$

$$M = -5.5\ z_c,$$

$$N = (5.5 - B)z_c,$$

$$P = -z_c(2B - 4.5 - \alpha_c)/2,$$

$$R = [1 + 5B]/[z_c(1 + B)^3] - 1,$$

$$S = [B(B - 3)]/[z_c(1 + B)^3], \text{ and}$$

where the subscript c corresponds to the critical state of the fluid and B is a function of the compressibility factor of the gas at the critical point, z_c,

$$z_c = \frac{B(3B - 1)}{(1 + B)^3} \quad . \qquad 7\text{-}11$$

The quantity α_c is the Reidel factor. Methods of calculating α_c are given in Reference 14.

To calculate a gas density ρ_g, an initial value is estimated based on Boyles law. This value is inserted into Eq. 7-9 and a value of z is calculated. This compressibility factor is used to calculate a better estimate of the gas density, and Eq. 7-9 is iterated until the compressibility factor changes less than 0.2% between two consecutive iterations. This value of the compressibility factor is used to calculate a final value for the gas density.

Temperatures

Various temperature differences associated with the heat pump cycle are given nominal values that are based on engineering judgment and overall cycle importance. For example, the condensate subcooling temperature

difference ($T_0 - T_1$) is assumed fixed for a given set of calculations, as is the suction superheat ($T_4 - T_3$) and the internal compressor temperature rise ($T_6 - T_5$). The temperature rise associated with the compression process is calculated based on the polytropic path equation and the ideal gas equation of state as

$$\frac{T_7}{T_6} = \left(\frac{P_7}{P_6}\right)^{(n-1)/n} \qquad 7\text{-}12$$

The temperatures T_5 and T_8 are calculated in an identical fashion using the pressure ratios P_5/P_4 and P_8/P_7, respectively.

Temperature T_9 is computed on the basis of an assumed heat retention between the compressor and discharge heat exchanger, which is a constant fraction of available superheat

$$T_9 = E_1 T_8 + (1 - E_1) T_{10} \qquad 7\text{-}13$$

where E_1 is the fraction of discharged superheat that reaches the condensor.

Enthalpy Balance

The total enthalpy gain on the suction side per unit mass is given by

$$\Delta H_{st} = (H_0 - H_1) + (H_3 - H_0) + (H_6 - H_3) \qquad 7\text{-}14$$

The suction-side enthalpy gain external to the compressor (i.e., neglecting compressor heating) is

$$\Delta H_{sp} = (H_0 - H_1) + (H_3 - H_0) + (H_4 - H_3) \qquad 7\text{-}16$$

The total enthalpy loss per unit mass on the condensor side of the circuit is

$$\Delta H_{ct} = (H_0 - H_1) + (H_3 - H_0) + (H_6 - H_3) + (H_7 - H_6). \qquad 7\text{-}16$$

The enthalpy change $(H_7 - H_6)$ is calculated using the enthalpy relation given in Eq. 7-6 for a reversible steady-flow process. A minimum number of enthalpy calculations are made on the high-pressure condensor side of the system. Since overall cycle closure allows use of either the input or output side of the heat pump cycle for enthalpy calculations, it was clear that the best choice at this level of modeling was to use the low-pressure evaporator side where compressibility effects were smaller and heat capacities of the vapor less pressure-dependent. The enthalpy loss per unit mass from heat transfer within the condensing heat exchanger is given by

$$H_{ce} = (H_0 - H_1) + (H_3 - H_0) + (H_6 - H_3) + (H_7 - H_6) - (H_8 - H_9). \qquad 7\text{-}17$$

Valve Pressure Drop

Pressure drop across the compressor inlet and outlet valves has been modeled using an empirical turbulent-flow friction factor,

$$\Delta P_{m,n} = \alpha_{m,n} \dot{m}^2$$

where $\dot{m}$ is the average mass flow rate through the valve. The parameter α is determined empirically from a curve-fit to experimental compressor data. As the model is presently configured, it is assumed that the pressure drops ΔP_{45} and ΔP_{78} are equal in value.

Computation of Heat Pump Balance Point

A two-level, nested iteration procedure was used to determine a stable operating point (see Figure 18). An initial guess of the saturated suction and discharge temperatures is made for given ambient and solar conditions.

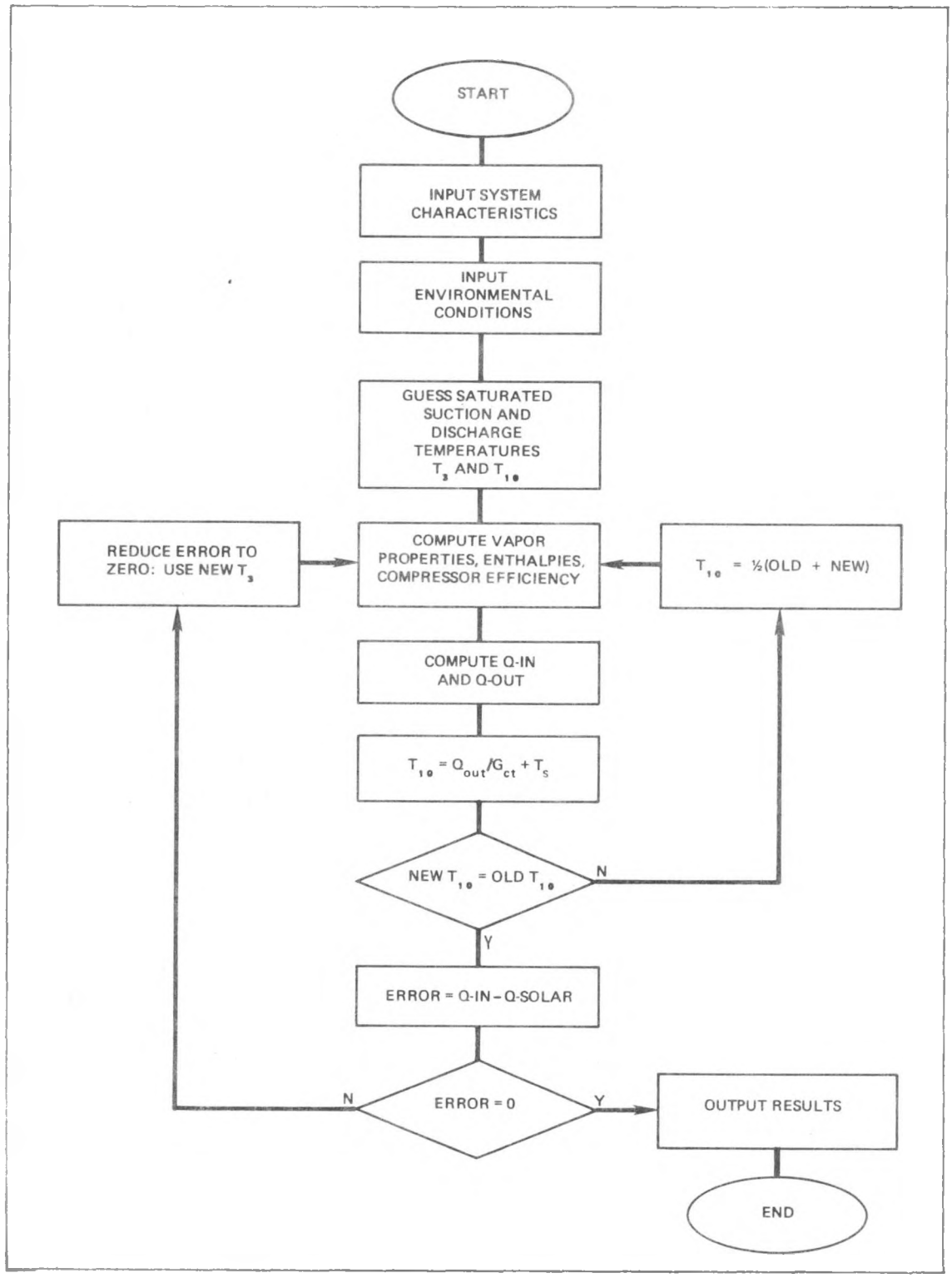

Figure 18. Flow Chart for Solar Heat Pump Modeling.

With the saturated suction and compressor mechanical characteristics defined and fixed, it is possible to calculate a unique saturated discharge temperature.

This value is used in the subsequent iteration to update high-side conditions, and a new discharge temperature value is calculated on the basis of heat output. The process is continued until the discharge temperature change is less than a given small value per iteration; then, it is assumed to be in satisfactory balance with the assumed saturated suction temperature.

At this point, the thermodynamically computed heat input is compared with available heat flux at the solar collector, and an adjusted suction temperature is calculated to bring these values into closer agreement. The iterative procedure discussed previously is used on the value of the saturated discharge temperature until its change between iterations reaches zero. When both discharge and suction temperatures stabilize, complete thermal equilibrium has been reached; the computed heat input equals the collector output for the stated solar flux, ambient temperature, system physical characteristics, wind velocity, and dew point; and the heat pump output flux is in thermal equilibrium with the thermal capabilities of the condensing heat exchanger/heat sink subsystem. A listing of the program SOLHP appears as Appendix C.

HEAT PUMP SOLAR HEATING COST ESTIMATES

To gain a perspective on collector costs and buy-back time, a reference collector system was defined and costed using the hybrid collector. To ensure that installation costs were as valid as possible, an independent construction firm, Levernier-Shea of Spokane, Washington, was requested to quote on installation of the reference collector. The collector array is shown schematically in Figure 19, and consists of an assembly of 10 collector rows. Each row is made from two 20-ft (6.1-m) lengths of 3/8-in. (0.95-cm) OD type-K copper tube with a 0.035-in. (0.089-cm) wall, and a 6-in. (15.2-cm) wide, 24-ga. (0.069-cm) copper collector fin.

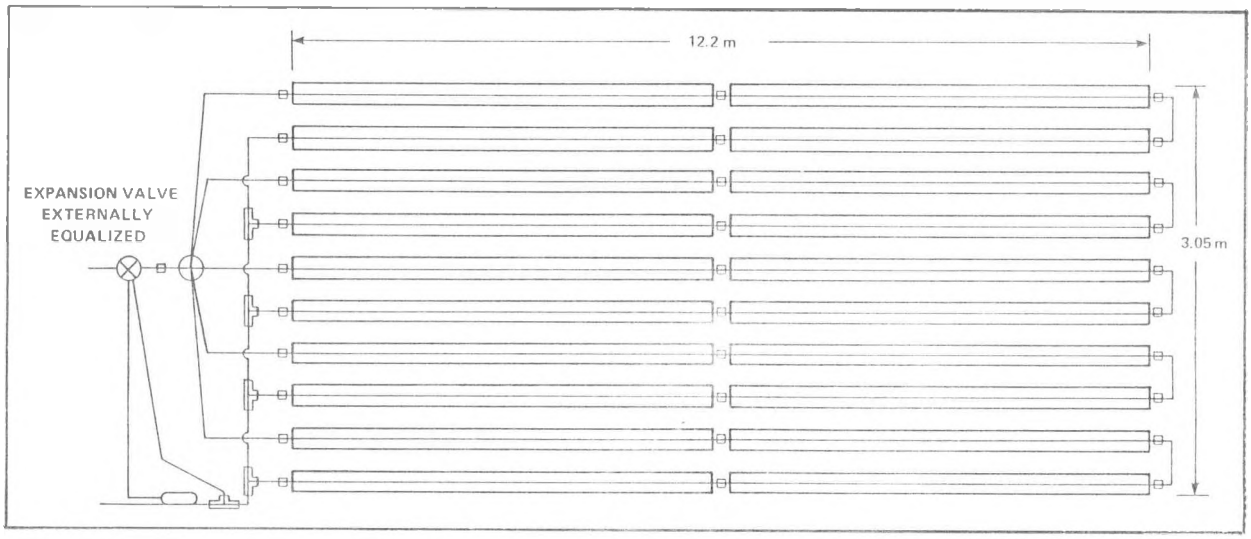

Figure 19. Piping Diagram for 37-m^2 Installation of Heat-Pumped Solar Collector.

For a 1:1 fin/gap spacing, the total collector roof area used is approximately 400 ft^2 (37.2 m^2). General system specifications are given in Table 6. Because the primary function is solar heating, only winter heating was considered although, for a small incremental cost, summer cooling could also be accomplished. Tables 7 through 10 detail this costing exercise, and Table 11 presents an overall summary of costs broken down for

- solar collector,
- heat pump module, and
- installation costs.

If the collection system alone is considered and the duct heater and heat exchanger are excluded, the installed collector cost (including the heat pump unit) is $8.30 per square foot. If the cost includes supplemental electric resistance heating and a duct-type condensing heat exchanger, installed system costs are about $10.50 per square foot of collector area. Typical installed solar collectors of conventional design cost approximately twice as much as these units (i.e., on the order of $18 to $20 per

Table 6

REFERENCE HEAT PUMP/SOLAR COLLECTOR DESIGN

Item	Dimension/Capacity	
	English	Metric
Overall Array Size (45° tilt, south-facing)	10 x 40 ft	3.05 x 12.1 m
Fin Material	14-ga copper	0.055-cm copper
Fin Width	6 in.	15.2 cm
Fin-to-Fin Gap	6 in.	15.2 cm
Fin Vertical Displacement From Roof	6 in.	15.2 cm
Roof Pitch (south-facing)	45°	N/A
Evaporator Tube Diameter (copper)	0.375 in. OD/0.305 ID	0.953 cm/0.775 cm
Individual Solar Panel Refrigerant Circuit Length	80 ft	24.4 m
Pressure Drop in Solar Panel Circuit*		
Suction Line OD per Pressure Drop**	7/8 in./1.8 psi	N/A
Discharge Line OD per Pressure Drop†	1/2 in./1.25 psi	N/A
Compressor Displacement, $\Delta P = 0$	7.5 CFM	3,540 cc/s
Compressor Clearance Factor	0.1	N/A
Condensing Heat Exchanger Conductance††	1,536 Btu/hr·°F	810 W/°C
Working Fluid	R-22	N/A
Lumped Heat Transfer Coefficient to Ambient	1.4 Btu/hr · ft^2-°F	0.8 mW/cm^2K
Solar Absorptivity (panel/white backing)	0.92/0.23	N/A
Infrared Absorptivity (panel/white backing)	0.92/0.85	N/A

*R-22, uniform evaporation, 50% vapor-liquid mixture, 40°F, 13 kW.

**50°F, 13 kW compressor capacity, 25 feet.

†80°F, 13 kW compressor capacity, 25 feet.

††Inlet saturated vapor-inlet air.

square foot) and have much lower collection efficiencies. The solar collection efficiency of this unit will range from 0.75 to more than 1.0, whereas the efficiency of conventional collectors would be on the order of 30-50%. Once again it must be noted that an apparent collection efficiency greater than 1.0 is possible because of heat input by convection and radiation from the surrounding ambient air when the panels are operated below ambient temperature.

Table 7

ON-SITE FULLY BURDENED LABOR COSTS

Trade	Total Hourly Cost
Carpenter	$18.00
Painter, Brush	18.25
Painter, Spray	18.67
Plumber or Steamfitter	25.00
Sheet Metal Worker	20.88
General Laborer	15.58
Electrician, Journeyman	20.77

A second system configuration was costed out and considered an ambitious homeowner who bought most of the collector materials and built the system with minimal help from professional laborers. In this scenario, it was assumed that the owner had built the collector panels and mounted them on his roof with free help, perhaps from a neighbor. The heat pump module was considered to be too sophisticated for a typical handyman to construct and was assumed to have been purchased as a unit. In addition, the soldering of refrigerant lines was assumed to have been performed by a plumber and electrical wiring by an electrician.

Under these boundary conditions, the system cost (including a duct heater and heat exchanger) was $7.50 per square foot--or a reduction of 28% in total cost. This amounts to a saving of $1,160 for a 400-$ft^2$ collector and is significant. A cost of $7.50 per square foot is lower than the purchase price of most uninstalled flat-plate collectors.

PREDICTED HOURLY PERFORMANCE-REFERENCE DESIGN

For the reference design discussed on page 62, Figure 20 shows the interrelationship of incident solar flux, heat output, and key system temperatures for a typical January day in Richland. The collector/

Table 8

COLLECTOR HARDWARE COSTS PER UNIT LENGTH*

Item	Comments	Dollars per Foot
Collector Plate	24-ga copper, 6-in. width	0.900
Collector Tube, 3/8 Type K	0.035-in. wall	0.269
Solder and Gas	solder = 0.032 lbs/ft	0.137
V-Brace Support Frame, 1/2 x 1/2 x 1/8 Carbon Steel	painted; 1 primer; 2 enamel	0.155
Mounting Brackets, 10-ft Spacing	painted	0.185
Tube Support Spacer, 2-ft Spacing, Plastic Extrusion	N/A	0.050
Refrigerant, Nominal 1/3 Liquid Fill	R-22	0.014
Primer, 1 Coat on Panels	$7.70/gal; 440 SF/gal	0.010
Flat Black Enamel on Panels, 2 Coats	$12.50/gal; 500 SF/gal	0.025
Row-to-Row 180° Bends	copper tube	0.010
2 x 4, 10 ft, 3 each	interface between mounting and brackets	0.023
Liquid Roofing and Caulking on 2 x 4's	Hypalon (TM)	0.076
Roofing Liquid, Applied	12 ft x 42 ft	**
Titanium White on Roofing	12 ft x 42 ft	**
Rough Hardware: Nails, Screws, etc.	N/A	0.050
Miscellaneous Sweat Fittings, Reducers (includes fittings up to compressor tees)	N/A	0.037
Total per Unit Length		$1.841
Total for 37-m^2 Collector		$736.40

*Assuming a collector plate of 24-ga copper, 6-in. (15.2-cm) wide.

**Part of building costs.

Table 9

HARDWARE COSTS EXCLUSIVE OF COLLECTOR*

Item	Comments	Cost
5-Ton Expansion Valve	Alco	$30.00
5-Outlet Capillary Distributor	N/A	8.00
7/8 Type-K Suction Line	15 ft	16.00
1/2 Type-K Liquid Line	15 ft	7.00
1/4 Type-K Liquid Line	35 ft	7.50
Refrigerant, Excluding Array	10 lbs, R-22	10.00
Compressor, 7.5 CFM	Copeland, Tecumseh	343.00
Fan-Coil Condenser With Houring	810 W/°C, including blower	320.00
Duct Heater	16 kW, 55 mBtu	238.00
Receiver, 1 each	7.7 lb	25.00
Solenoid Valve, 3 each	5-ton	66.00
Dryer, 1 each	N/A	18.00
Moisture Indicator	N/A	12.00
High-Pressure Cut-Out	Penn Controls	22.00
Electrical Controls	N/A	38.00
Heat Pump Enclosure, Switch Box	sheet metal, painted	55.00
Miscellaneous Charging Valves, Fitting, Tubing	N/A	30.00
	TOTAL	$1,186.50

*Based on a heating-only heat pump and neglecting solar storage tank. Hardware is at contractor cost.

Table 10

LABOR COSTS FOR MANUFACTURE OF COMPONENTS AND INSTALLATION OF HYBRID SOLAR HEATING SYSTEM

Item	Labor Rate/Time	Cost
SOLAR COLLECTORS:		
Solder Tube to Collector Plate	sheet metal worker/40 s per ft	$0.232*
Prepare for Painting	general laborer/20 s per ft	0.987
Paint Tube/Plate Assembly	spray painter/10 s per ft 1 coat primer, 2 coats enamel	0.156
Paint V-Brace Support Frame		0.27
Miscellaneous Shearing, Cutting, Inspection, Crating		0.100
	Total Labor to Manufacture Collector	$0.602*
	Total for 37-m^2 Collector	$240.80
HEAT PUMP MODULE		
Component Assembly	electrical, steam fitter/8 manhours	$183
INSTALLATION		
Attach 2 x 4's, 3 each, to Roof	carpenter/0.5 hr	$9.00
Caulk Under 2 x 4's	carpenter/$2 per linear foot	12.00
Apply Liquid Roofing Over 2 x 4's	carpenter/0.75 hr	13.50
Assume Crew of 2, Layout and Fabricate 4 ft x 20 ft and 2 ft x 20 ft Units on Ground. Total of 6 Assemblies—Assume 8 Hours Each.	carpenter	288.00
To Lift to Roof—Assume 4 Hours for Small Crane or Cherry-Picker (including travel to and from)	4 hours @ $30 per hour	120.00
Labor Crew for Above	carpenter/8 manhours	144.00
Install Units on Roof—Assume 2 Men for Half Day	carpenter/8 manhours	144.00
Plumbing Labor Costs to Make Connections Back to Distribution Block—Assume 1 Plumber for 8 Hours to Complete Work	plumber/8 manhours	200.00
Installation of Duct Direct Condensation Coil and Supplemental Heater	plumber/4 manhours and electrician/4 manhours	183.00
Charging and Start-Up of System; Install Wiring and Thermostat	plumber/4 manhours and electrician/4 manhours	183.00
	Installation Costs	$1296.50

*Per foot.

Table 11

COST SUMMARY FOR 37-m^2 HYBRID HEAT-PUMPED SOLAR HEATING SYSTEM

Item		Dollars/ft^2 of Collector Area	Cost to Consumer*
REFERENCE DESIGN**:			
Solar Collector (materials plus labor)		$2.93	$1,172.64
Heat Pump Module† (materials pus labor)		2.61	1,044.60
Installation (primarily labor)		2.78	1.113.50
	TOTAL	$8.32	$3.330.74
ALTERNATE 1†		$10.46	$4,183.34
ALTERNATE 2††			
Solar Collector (materials)		$1.84	$736.40
Heat Pump Module (materials plus labor)		4.29	1,714.20
Installation (plumber and electrician)		1.42	566.00
	TOTAL	$7.55	$3,016.60

*Assuming a 20% markup by solar manufacturer and direct sale to consumer.

**Costs of collection system only; i.e., neglecting any duct heat exchanger or associated labor.

+Includes miscellaneous piping, direct expansion duct heat exchanger, and 16 kW supplemental heating but not solar storage.

††Same as Alternate 1 except for an ambitious homeowner who builds his own collector array and who purchases at markup only the heat pump module. A plumber and electrician are still assumed necessary for final installation and soldering of refrigerant lines.

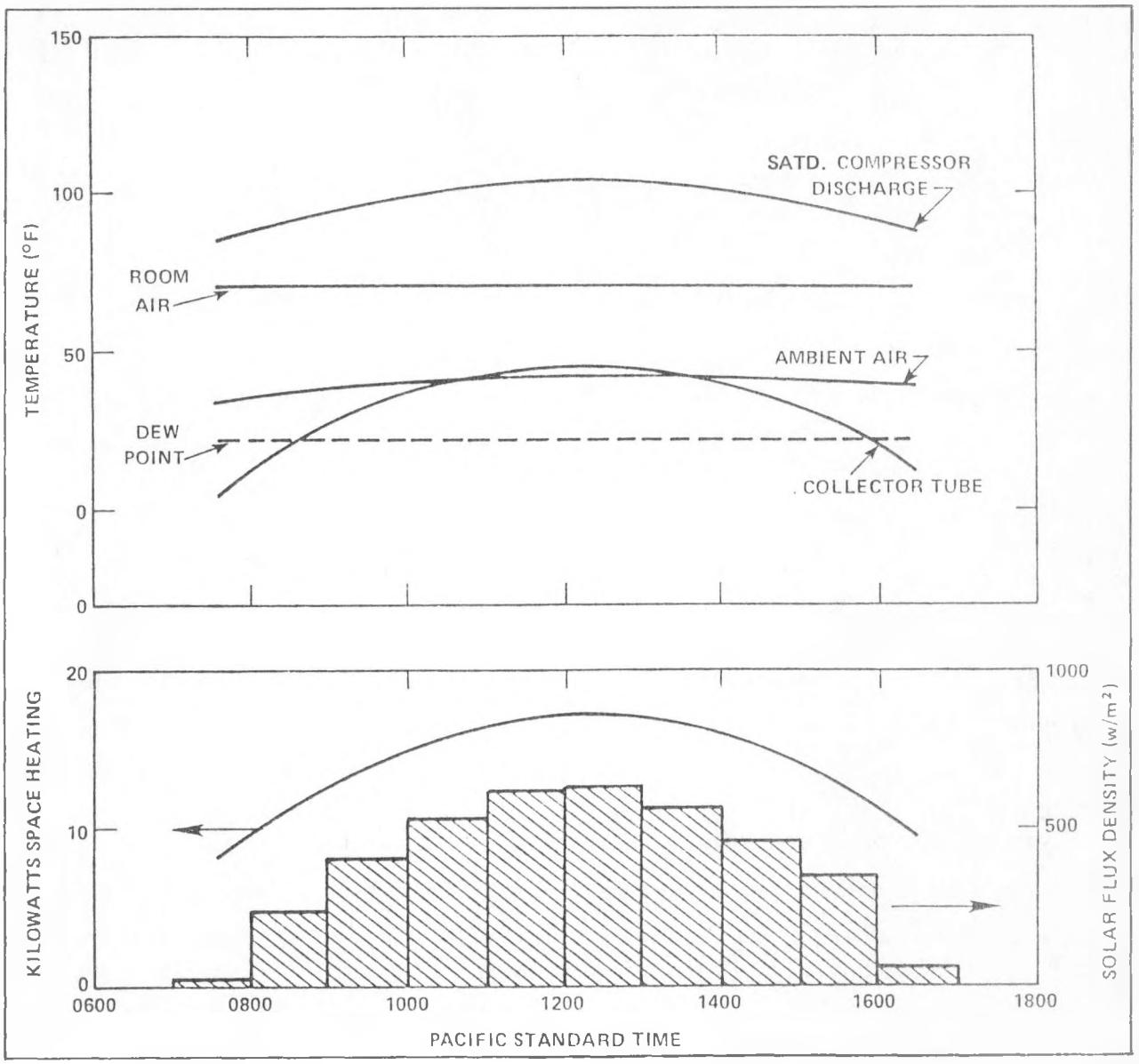

Figure 20. Response of Reference Solar Heat Pump on Average January Day in Richland. (Climatological conditions are very similar to a clear day in Seattle.)

evaporator tube on the panel fluctuates from 10°F to 45°F (-12°C to 7.2°C) over a solar day, while the saturated compressor discharge varies from 80°F to 104°F (29°C to 40°C), respectively. The climatological conditions used here closely parallel a clear January day in Seattle.

On the other hand, an average day in Seattle is relatively cloudy and the dew point is about 33°F (0.6°C). This cloudy condition may not degrade collector performance as much as might initially be expected because of the enhanced heat transfer associated with condensation on the panels. It is quite clear that the exposed panel would fare better than the glazed panel, since the solar collection efficiency of an exposed panel does not drop with decreasing solar flux.

Table 12 presents system COP for the reference design under January conditions in Richland. An overall COP of 3.55 is shown, and this relatively high value is due in part to the absence of an evaporator fan and in part to the higher mean evaporating temperature attributable to solar absorption. A conventional heat pump would, in general, always display a lower heating COP for these two reasons.

A COMPARISON WITH FLAT-PLATE COLLECTORS

On page 63 it was shown that a solar heat pump system has an installed cost in the range of $8 to $10 per square foot. This value is approximately a factor of two lower than installed conventional flat-plate collectors, but the comparison is actually incomplete until relative thermal performance is factored in. The major failing of existing solar hardware is not expense but a poor return on investment (ROI). If a solar collector is costly but very efficient, it may be a good investment; a costly, inefficient collector is never a good buy.

For an economic comparison of heat pumps and flat-plate systems, a model based on buy-back time was used. Buy-back times for solar installations are typically quite long; hence, a reduction in this factor is desirable to establish widespread use of solar energy. If it is assumed that a standard, electrically heated home has an annual heating cost, E, the addition of a solar collector-heat pump system will yield an annual cost, C_A, which is given by

Table 12

HEATING COEFFICIENT OF PERFORMANCE FOR REFERENCE SOLAR HEAT PUMP ON AN AVERAGE JANUARY DAY IN RICHLAND, WASHINGTON*

Time (PST)	Space Heating (W)	Compressor Plus Fan Input (W)	Overall COP
0730	8,357	3,223	2.59
0830	11,156	3,567	3.13
0930	13,465	3,806	3.54
1030	15,483	3,992	3.88
1130	16,713	4,093	4.08
1230	17,048	4,120	4.14
1330	16,270	4,056	4.01
1430	14,877	3,936	3.78
1530	13,099	3,770	3.47
1630	9,596	3,386	2.83
	136**		3.55†

*Overall heating COP = heat output divided by compressor plus air circulator fan electrical input. Condensing heat exchanger uses ½-hp fan, 725-W dissipation. Compressor mechanical system and motor approximately 60% efficient. See Table 2 for weather conditions.

**kW-hr.

†Average.

$$C_A = \left[1 - \eta_{hp}\left(1 - \frac{1}{COP_{hp}}\right)\right] E + \left[\left(P_{hp}\right)\left(F_N\right)\right] \quad , \qquad 7\text{-}18$$

where:

η_{hp} = fraction of space heating delivered by the system,

P_{hp} = initial system cost,

COP_{hp} = overall heating coefficient of performance, and

F_N = buy-back factor,

which relates equipment life and the time value of money to a uniform yearly capital equipment operating burden. At the break-even point ($E = C_A$), rearrangement yields

$$F_N = \left[\frac{\eta_{hp} E \left(1 - \frac{1}{COP_{hp}} \right)}{P_{hp}} \right] \qquad 7\text{-}19$$

In this equation, F_N is actually the yearly ROI, and a large value of F_N is desirable to minimize buy-back time. If the same analysis is performed for a flat-plate system, the ratio between ROI's is an indication of relative cost-effectiveness

$$F^+ = \frac{\text{ROI for heat pump}}{\text{ROI for flat plate}} = \frac{\eta_{hp} P_{fp}}{\eta_{fp} P_{hp}} \left[\frac{\left(1 - \frac{1}{COP_{hp}} \right)}{\left(1 - \frac{1}{COP_{fp}} \right)} \right] \qquad 7\text{-}20$$

where the subscript fp represents flat plate.

If the thermal comparison is done for an average January day in Richland, as on page 72, about 136 kW-hr of energy are generated at a COP of 3.55 (see Table 12) for the reference heat pump system. Alternatively, for Revere flat-plate collectors to operate at the average heat pump condenser temperature of 96°F (35.6°C) with an average air temperature of 39.7°F (4.3°C) and at a nominal solar flux density of 122 Btu/hr-ft^2 (384 W/m^2), a maximum efficiency of 41% is indicated in their publication, "13.25/Re." Therefore, for a 37-m^2 (400-ft^2) collector as used in the reference design, the absorbed energy is on the order of 58.6 kW-hr. Per conversations with D. Boleyn concerning the Portland General Electric Boleyn solar house, installed collector cost was found to be approximately $18 per square foot, exclusive of thermal storage, heat exchangers, and supplemental heating.

With these numbers, the relative returns on investment are

$$F^{+} = \frac{\left(136\right)\left(18\right)\left(1 - \frac{1}{3.55}\right)}{\left(58.6 + 7.25\right)\left(9\right)\left(1 - \frac{1}{9.1}\right)} = 3.33 \qquad 7\text{-}21$$

where allowance has been made for a 1/2-hp duct fan. Therefore, under these winter conditions, the heat pump system will pay for itself at three times the rate of the Revere flat-plate collector.

BUY-BACK TIME

Using climatological data for the Richland area (Tables 3 and 4), yearly fuel savings were calculated for the reference 37-m^2 (400-ft^2) collector and heat pump system described in previous sections. For this purpose, the building to be heated was modeled as a lumped system with a heat loss to ambient of 604 W/°C temperature difference. In Richland, this corresponds to a maximum yearly peak heating requirement of about 16 kW (55 MBtu/hr). This particular heating load was selected so that the reference hybrid solar heating system would contribute about 70% of the yearly space heating requirement.

The performance of this building and heating system combination is summarized in Table 13. To compensate for deterioration of the reflective backing, possible frost-cover effects, and snow cover, the heat pump was assumed to operate for only 90% of the solar day. Thermal storage was assumed available so that, on a monthly basis, all collected energy not in excess of building needs was used (i.e., if the heat pump can supply 6,000 kW-hr of energy in the month of April but the building can only use 2,500 kW-hr, the excess 3,500 kW-hr are neglected). Maximum monthly heat output of the collector system was calculated by integrating hourly performance data, using monthly hourly average insolations and temperatures, and multiplying by the number of days in that specific month. With these stipulations, the heat pump collector system provides 72% of the yearly heating

Table 13

YEARLY HEATING PERFORMANCE SUMMARY

Month	Degree-Days	Heating Energy Needed/Month (kW-hr)	Maximum Energy Available From Solar Heat Pump* (kW-hr)	Total Electrical Input*/COP	Electrical Demand to Satisfy Heating Heating Load (kW-hr)
Jan	965	8,227	3,796	1,059/3.58	1,059
Feb	679	5,788	4,461	1,262/3.53	1,262
Mar	569	4,851	5,820	1,418/4.10	1,183
Apr	292	2,489	6,255	1,495/4.18	595
May	128	1,091	7,321	,763/4.15	263
Jun	–	–	–	–	–
Jul	–	–	–	–	–
Aug	–	–	–	–	–
Sep	50	426	6,915	1,549/4.46	96
Oct	293	2,498	5,785	1,342/4.31	579
Nov	633	5,396	4,232	1,113/3.80	1,113
Dec	865	7,374	3,555	1,007/3.53	1,007
	4,474 °F Days	38,140 kW-hr	27,399 kW-hr**		7,157 kW-hr
					Avg COP = 3.83

*Value displayed is 10% lower than actual calculated value to compensate for defrost cycles, etc.

**Equals usable heat not in excess of demand (72% of heating load).

needs at a heating COP of 3.83. The yearly ROI for this system is given by Eq. 7-19,

$$ROI = \frac{\eta_{hp} \, E \left(1 - \frac{1}{COP_{hp}}\right)}{P_{hp}}$$

If the cost of electric heating is 3¢/kW-hr, the ROI for this particular system--when a duct heat exchanger and 16-kW supplemental heating are included--is

$$\text{ROI} = \frac{0.72\left[\left(0.03\right)\left(38,\ 140\right)\right]\left[1 - \frac{1}{3.83}\right]}{4183} = 0.146\ \text{yr}^{-1}$$

The buy-back time is the inverse of ROI when the time values of money, inflation, etc., are neglected; hence

$$\text{the system pays for itself @ 3¢/kW-hr in } \frac{1}{0.146}\ \text{yr} = 6.9\ \text{yr}.$$

It must be noted, of course, that the total buy-back time will be somewhat longer because the thermal storage system has not been included in system cost although its benefits have been assumed.

The basic fact that stands out is that the specific heating-only system configured here will have a buy-back time of less than approximately 10 years without attaching any value to possible summer cooling.

Section 7

REFERENCES

1 J. Duffie and W. Beckman, Solar Energy Thermal Processes, Wiley and Sons, New York, 1974.

2 Solar Energy Heat Pump Systems for Heating and Cooling Buildings, S. F. Gilman (ed.), ERDA Document C00-2560-1, 1975.

3 P. I. Cooper, "The Absorption of Solar Radiation in Solar Stills," Solar Energy, 12, 1969, p. 3.

4 W. M. Smart, Text Book on Spherical Astronomy, 5th ed., Cambridge University Press, 1971.

5 W. M. Kays, Convective Heat and Mass Transfer, McGraw-Hill, New York, 1966.

6 F. Krieth, Principles of Heat Transfer, Int. Textbook Co., Scranton, PA, 1967.

7 R. B. Bird, W. E. Stewart, and E. D. Lightfoot, Transport Phenomena, Wiley and Sons, New York, 1960, pp. 572-574.

8 C. O. Bennett and J. E. Myers, Momentum Heat and Mass Transfer, 2nd ed., McGraw-Hill, New York, 1974.

9 R. C. Reid, J. M. Pravsnitz, and T. K. Sherwood, The Properties of Gases and Liquids, 3rd. ed., McGraw-Hill, New York, 1977, pp. 181-184.

10 B. G. Levich, Physiochemical Hydrodynamics, Prentice-Hall, Inc., Englewood Cliffs, NJ, 1970.

11 Compressors: Application Data, Expanded Ratings, Carrier Corp., ASME Pub. 80-WA/S01-32, 1967.

12 Air Conditioning Refrigerating Data Book, American Society of Refrigerating Engineers, Menasha, WI, 1955, Tables 22 and 23.

13 J. L. Threlkeld, Thermal Environmental Engineering, Prentice-Hall, Inc., Englewood Cliffs, NJ, 1970.

14 R. C. Reid and T. K. Sherwood, The Properties of Gases and Liquids, McGraw-Hill, New York, 1966.

Appendix A

MODELING PROGRAM VIEW

This program computes view factors for direct and reflected illumination of a collector system given its geometry and the position of the sun.

```
_w    11:01 AM        18-Sep-79
10 INPUT "BACKING WIDTH";L1
30 INPUT "LENGTH OF ROOF IN FRONT OF BACKING";L2
50 INPUT "DISTANCE TO LOWER EDGE OF FIN";H1
70 INPUT "WIDTH OF FIN";W1
90 INPUT "SPACING BETWEEN FINS";W2
110 INPUT "DISTANCE BETWEEN FIN AND BACKING";D
130 INPUT "ANGLE OF BACKING TO ROOF -DEGREES-";T
150 INPUT "ALTITUDE OF SUN -DEGREES-";G
170 INPUT "AZIMUTH OF SUN -DEGREES-";J
190 P = 3.14159
200 T = T*P/180
210 G = G*P/180
220 J = J*P/180
225 G = ATN(TAN(G)/COS(J)) ! PROJECTED SHADOW ANGLE
226 IF G<0 THEN G = P-G
230 ! VIEW FACTORS ARE CALCULATED BY HOTTEL'S METHOD. FINS, BACKING, ETC.
    ARE ASSUMED TO BE INFINITELY LONG.
240 X1 = H1*COS(T) - D*SIN(T)
250 X2 = (H1+W1)*COS(T) - D*SIN(T)
260 Y1 = H1*SIN(T) + D*COS(T)
270 Y2 = (H1+W1)*SIN(T) + D*COS(T)
275 ! X1,Y1 AND X2,Y2 ARE THE LOCATIONS OF THE LOWER AND UPPER EDGES OF THE FIN
280 X3 = L1*COS(T)
290 Y3 = L1*SIN(T)
295 ! X3,Y3 IS THE LOCATION OF THE UPPER EDGE OF THE BACKING
310 V = (P/2 - T) - G
320 ! V IS THE ANGLE BETWEEN THE SUN'S RAYS AND THE NORMAL TO THE COLLECTOR'S
    SURFACE.
330 S = D*TAN(V)
340 X4 = (H1+S)*COS(T)
350 Y4 = (H1+S)*SIN(T)
360 IF X4>=0 GO TO 410
370 IF X4>=0 GO TO 460
380 X4 = X4 + (W1 + W2)*COS(T)
390 Y4 = Y4 + (W1 + W2)*SIN(T)
400 GO TO 370
410 X = X4 - (W1 + W2)*COS(T)
420 IF X<0 GO TO 460
430 X4 = X
440 Y4 = Y4 - (W1 + W2)*SIN(T)
450 GO TO 410
460 ! X4,Y4 IS NOW THE LOCATION OF THE LOWEST UPPER SUN LIT EDGE
470 Z = H1 + W1
480 IF Z>L1 THEN PRINT "FIN OVERLAPS UPPER EDGE OF BACKING"
490 Z1 = Z + W1 + W2
500 IF Z1>L1 GO TO 530
510 Z = Z1
520 GO TO 490
530 X5 = Z*COS(T) - D*SIN(T)
540 Y5 = Z*SIN(T) + D*COS(T)
550 ! X5,Y5 IS THE LOCATION OF THE UPPER EDGE OF THE UPPER FIN
560 A = FIX((Z + W2)/(W1 +W2))
570 PRINT "TOTAL NUMBER OF FINS = "A
580 X6 = X5 - (A*(W1 + W2) - W2)*COS(T)
590 Y6 = Y5 - (A*(W1 + W2) - W2)*SIN(T)
600 ! X6,Y6 IS THE LOCATION OF THE LOWER EDGE OF THE LOWER FIN
610 X7 = X5 + D*SIN(T) + S*COS(T)
620 Y7 = Y5 - D*COS(T) + S*SIN(T)
630 IF X7<=X3 GO TO 670
```

```
640 X7 = X7 - (W1 + W2)*COS(T)
650 Y7 = Y7 - (W1 + W2)*SIN(T)
660 GO TO 630
670 ! X7,Y7 IS THE LOCATION OF THE LOWER EDGE OF THE UPPER SUN LIT BAND
      NOTE: THE UPPER EDGE OF THE UPPER SUN LIT BAND IS EITHER THE UPPER
      EDGE OF THE BACKING OR A DISTANCE W2 AWAY FROM THE LOWER EDGE OF THE
      UPPER SUN LIT BAND.
680 X8 = -D/SIN(T)
690 Y8 = 0
700 ! X8,Y8 IS THE LOCATION OF THE INTERSECTION OF THE PLANE OF THE FINS
      AND THE PLANE OF THE ROOF.
710 X9 = -L2
720 Y9 = 0
730 ! X9,Y9 IS THE LOCATION OF THE EDGE OF THE ROOF
740 F1 = ((SQR((X2-X8)**2 + (Y2-Y8)**2) + SQR((X1-X9)**2 + (Y1-Y9)**2))
    - (SQR((X1-X8)**2 + (Y1-Y8)**2) + SQR((X2-X9)**2 + (Y2-Y9)**2)))/(2*W1)
750 PRINT "VIEW FACTOR -FRONT OF FIN TO ROOF- ="F1
760 D = -1.0E+6
765 ! D,0 IS THE LOCATION OF THE HORIZON
770 F2 = ((SQR((X1-D)**2 + Y1**2) + SQR((X2-X9)**2 + Y2**2)) -
          (SQR((X1-X9)**2 + Y1**2) + SQR((X2-D)**2 + Y2**2)))/(2*W1)
780 PRINT "VIEW FACTOR -FRONT OF FIN TO TERRAIN- ="F2
790 F3 = ((SQR((X2-D)**2 + Y2**2) + SQR((X1-X5)**2 + (Y1-Y5)**2))-
          (SQR((X1-D)**2 + Y1**2) + SQR((X2-X5)**2 + (Y2-Y5)**2)))/(2*W1)
800 PRINT "VIEW FACTOR -FRONT OF FIN TO SKY- ="F3
810 PRINT "SUMMATION OF VIEW FACTORS ="F1+F2+F3
820 F4 = ((SQR((X1-X3)**2 + (Y1-Y3)**2) + SQR(X2**2 + Y2**2)) -
          (SQR(X1**2 + Y1**2) + SQR((X2-X3)**2 + (Y2-Y3)**2)))/(2*W1)
830 PRINT "VIEW FACTOR -REAR OF FIN TO BACKING- ="F4
840 F5 = ((SQR(X1**2 + Y1**2) + SQR((X2-X8)**2 + (Y2-Y8)**2)) -
    (SQR((X1-X8)**2 + (Y1-Y8)**2) + SQR(X2**2 + Y2**2)))/(2*W1)
850 PRINT "VIEW FACTOR -REAR OF FIN TO ROOF- ="F5
860 F6 = ((SQR((X1-X5)**2 + (Y1-Y5)**2) + SQR((X2-X3)**2 + (Y2-Y3)**2)) -
    (SQR((X1-X3)**2 + (Y1-Y3)**2) + SQR((X2-X5)**2 + (Y2-Y5)**2)))/(2*W1)
870 PRINT "VIEW FACTOR -REAR OF FIN TO SKY- ="F6
880 PRINT "SUMMATION OF VIEW FACTORS ="F4+F5+F6
885 IF Y2<=Y3 GO TO 890
886 PRINT "***** A PORTION OR ALL OF THIS FIN VIEWS THE TERRAIN BEHIND THE BACKI
NG *****"
890 IF X4>X7 THEN PRINT "ENTIRE BACKING SUN LIT" : GO TO 1080
900 U1 = X7 + W2*COS(T)
910 V1 = Y7 + W2*SIN(T)
920 IF U1>X3 THEN U1=X3: V1=Y3
930 !U1,V1 IS THE LOCATION OF THE UPPER EDGE OF THE UPPER SUN LIT BAND
940 F7 = 0: N = 0
950 F7 = F7  + ((SQR((X1-U1)**2 + (Y1-V1)**2) + SQR((X2-X7)**2 + (Y2-Y7)**2))
    -(SQR((X1-X7)**2 +(Y1-Y7)**2) + SQR((X2-U1)**2 + (Y2-V1)**2)))/(2*W1)
960 X7 = X7 - (W1 + W2)*COS(T)
970 Y7 = Y7 - (W1 + W2)*SIN(T)
980 U1 = X7 + W2*COS(T)
990 V1 = Y7 + W2*SIN(T)
995 !X7,Y7 IS THE LOCATION OF THE LOWER EDGE OF THE SUN LIT BAND BEING CAL
     CULATED AND U1,V1 IS THE LOCATION OF THE UPPER EDGE OF THE SUN LIT BAND
     BEING CALCULATED
1000 N = N + 1
1010 IF X7<0 THEN X7=0: Y7=0
1020 IF U1<0 GO TO 1040
1030 GO TO 950
1040 PRINT "NUMBER OF SUN LIT BANDS ="N
1050 PRINT "VIEW FACTOR -REAR OF FIN TO SUN LIT BACKING- ="F7
1060 F8 = F4 - F7
1070 PRINT "BY DIFFERENCE  VIEW FACTOR -REAR OF FIN TO SHADED BACKING- ="F8
```

```
1080 U2 = X6 + Y6/TAN(G)
1090 !  U2,0 IS THE LOCATION OF SHADOW PROJECTED BY THE LOWER EDGE OF THE
       LOWEST FIN ON THE PLANE OF THE ROOF
1100 IF U2<=0 GO TO 1110
1105 PRINT "ALL OF THE ROOF VIEWED BY THE REAR FACE OF THE FIN IS SUN LIT"
1106 GO TO 1200
1110 U3 = U2 + W1*COS(T)
1120 IF U3<0 THEN PRINT "MULTIPLE SUN LIT BANDS ON ROOF VIEWED BY REAR OF FIN"
1125 IF U3<0 GO TO 1200
1130 U4 = X6 + W1*COS(T)
1140 V4 = Y6 + W1*SIN(T)
1150 !U4,V4 IS THE LOCATION OF THE UPPER EDGE OF THE LOWEST FIN
1160 F9 = ((SQR((X1-U2)**2 + Y1**2) + SQR((X2-X8)**2 + Y2**2)) -
     (SQR((X2-U2)**2 + Y2**2) + SQR((X1-X8)**2 + Y1**2)))/(2*W1)
1170 PRINT "VIEW FACTOR -REAR OF FIN TO SUN LIT PORTION OF ROOF- ="F9
1180 F = F5 - F9
1190 PRINT "BY DIFFERENCE  VIEW FACTOR -REAR OF FIN TO SHADED PORTION OF ROOF- =
"F
1200 END

Ready
```

Appendix B

MODELING PROGRAM SINPT

```
LIST
SINPT   11:36 AM        01-Sep-81
1 ! THIS PROGRAM CALCULATES THE TOTAL SOLAR INPUT TO A FIN (WATT-HOURS PER
METER SQUARED PER DAY).  THIS IS THE SUM OF THE DIRECT RADIATION TO THE FIN
PLUS REFLECTED TO THE FRONT PLUS RELECTED TO THE REAR.  NO INFRARED INPUTS
OR LOSSES HAVE BEEN TREATED.
5 P = 3.141592654
10 DEF FNC(X) = P/2 - ATN(X/SQR(1-X*X)) ! ARCCOS
11 DEF FNC1(X) = ATN(X/SQR(1-X*X)) ! ARCSIN
15 INPUT "DAY OF THE YEAR";N1
20 INPUT "LATITUDE";L
25 L = L*P/180
30 D1 = (23.45*P/180)*SIN(2*P*(N1+284)/365)
35 PRINT "SOLAR DECLINATION"D1*180/P
40 INPUT "ATMOSPHERIC TRANSMITTANCE";R
45 INPUT "BACKING LENGTH";L1
50 INPUT "BACKING REFLECTANCE";R1
55 INPUT "LENGTH OF ROOF IN FRONT OF COLLECTOR";L2
60 INPUT "ROOF REFLECTANCE";R2
65 INPUT "DISTANCE TO LOWER EDGE OF FIN";H1
70 INPUT "WIDTH OF FIN";W1
71 INPUT "FIN ABSORPTANCE";A9
75 INPUT "SPACING BETWEEN FINS";W2
80 INPUT "DISTANCE BETWEEN FIN AND BACKING";D
85 INPUT "ANGLE OF BACKING TO ROOF";T
90 T = T*P/180
95 I1 = FNC(-TAN(L)*TAN(D1)) ! HOUR ANGLE AT SETTING
100 S8 = 12 - I1*24/(2*P)
105 S9 = 12 + I1*24/(2*P)
110 PRINT "SUNRISE"S8"SUNSET"S9
115 M = -FNC((SIN(D1)*COS(L)*SIN(T) - SIN(D1)*SIN(L)*COS(T))/
        (COS(D1)*COS(L)*COS(T) + COS(D1)*SIN(L)* SIN(T)))
120 S6 = 12+M*24/(2*P)
125 S7 = 12-M*24/(2*P)
130 PRINT "ANGLE OF INCIDENCE IS 90 DEGREES AT"S6"AND"S7
135 IF S8>S6 THEN I2=S8 : I3=S9
140 IF S8<=S6 THEN I2=S6 : I3=S7
145 PRINT "INTEGRATION FROM"I2"TO"I3
150 T1 = (12-I2)/10
151 Q1=0:Q2=0:Q3=0
155 FOR K = 12+T1/2 TO 12-T1/2+.01 STEP T1
160 H = (12-K)*P/12
165 Z2 = FNC(SIN(L)*SIN(D1) + COS(L)*COS(D1)*COS(H)) ! ZENITH ANGLE
170 A1 = P/2 - Z2 ! ALTITUDE
175 B = P - FNC((SIN(D1) - SIN(L)*COS(Z2))/(COS(L)*SIN(Z2))) ! AZIMUTH
180 G = ATN(TAN(A1)/COS(B)) ! PROJECTED SHADOW ANGLE
185 IF G<0 THEN G = P+G
230 ! VIEW FACTORS ARE CALCULATED BY HOTTEL'S METHOD.  FINS, BACKING, ETC.
    ARE ASSUMED TO BE INFINITELY LONG.
240 X1 = H1*COS(T) - D*SIN(T)
250 X2 = (H1+W1)*COS(T) - D*SIN(T)
260 Y1 = H1*SIN(T) + D*COS(T)
270 Y2 = (H1+W1)*SIN(T) + D*COS(T)
275 ! X1,Y1 AND X2,Y2 ARE THE LOCATIONS OF THE LOWER AND UPPER EDGES OF THE FIN
280 X3 = L1*COS(T)
290 Y3 = L1*SIN(T)
295 ! X3,Y3 IS THE LOCATION OF THE UPPER EDGE OF THE BACKING
310 V = (P/2 - T) - G
320 ! V IS THE ANGLE BETWEEN THE SUN'S RAYS AND THE NORMAL TO THE COLLECTOR'S
    SURFACE.
330 S = D*TAN(V)
340 X4 = (H1+S)*COS(T)
350 Y4 = (H1+S)*SIN(T)
360 IF X4>=0 GO TO 410
370 IF X4=0 GO TO 400
380 X4 = X4 + (W1 + W2)*COS(T)
390 Y4 = Y4 + (W1 + W2)* SIN(T)
400 GO TO 370
```

```
410 X = X4 - (W1 + W2)*COS(T)
420 IF X<0 GO TO 460
430 X4 = X
440 Y4 = Y4 - (W1 + W2)*SIN(T)
450 GO TO 410
460 ! X4,Y4 IS NOW THE LOCATION OF THE LOWEST UPPER SUN LIT EDGE
470 Z = H1 + W1
480 IF Z>L1 THEN PRINT "FIN OVERLAPS UPPER EDGE OF BACKING"
490 Z1 = Z + W1 + W2
500 IF Z1>L1 GO TO 530
510 Z = Z1
520 GO TO 490
530 X5 = Z*COS(T) - D*SIN(T)
540 Y5 = Z*SIN(T) + D*COS(T)
550 ! X5,Y5 IS THE LOCATION OF THE UPPER EDGE OF THE UPPER FIN
560 A = PI*(Z + W2)/(W1 +W2)
580 X6 = X5 - (A*(W1 + W2) - W2)*COS(T)
590 Y6 = Y5 - (A*(W1 + W2) - W2)*SIN(T)
600 ! X6,Y6 IS THE LOCATION OF THE LOWER EDGE OF THE LOWER FIN
610 X7 = X5 + D*SIN(T) + S*COS(T)
620 Y7 = Y5 - D*COS(T) + S*SIN(T)
630 IF X7<=X3 GO TO 670
640 X7 = X7 - (W1 + W2)*COS(T)
650 Y7 = Y7 - (W1 + W2)*SIN(T)
660 GO TO 630
670 ! X7,Y7 IS THE LOCATION OF THE LOWER EDGE OF THE UPPER SUN LIT BAND
      NOTE: THE UPPER EDGE OF THE UPPER SUN LIT BAND IS EITHER THE UPPER
      EDGE OF THE BACKING OR A DISTANCE W2 AWAY FROM THE LOWER EDGE OF THE
      UPPER SUN LIT BAND.
680 X8 = -D/SIN(T)
690 Y8 = 0
700 ! X8,Y8 IS THE LOCATION OF THE INTERSECTION OF THE PLANE OF THE FINS
      AND THE PLANE OF THE ROOF.
710 X9 = -L2
720 Y9 = 0
730 ! X9,Y9 IS THE LOCATION OF THE EDGE OF THE ROOF
740 F1 = ((SQR((X2-X8)**2 + (Y2-Y8)**2) + SQR((X1-X9)**2 + (Y1-Y9)**2))
    - (SQR((X1-X8)**2 + (Y1-Y8)**2) + SQR((X2-X9)**2 + (Y2-Y9)**2)))/(2*W1)
750 D = -1.0E+6
765 ! D,0 IS THE LOCATION OF THE HORIZON
770 F2 = ((SQR((X1-D)**2 + Y1**2) + SQR((X2-X9)**2 + Y2**2)) -
         (SQR((X1-X9)**2 + Y1**2) + SQR((X2-D)**2 + Y2**2)))/(2*W1)
790 F3 = ((SQR((X2-D)**2 + Y2**2) + SQR((X1-X5)**2 + (Y1-Y5)**2))-
         (SQR((X1-D)**2 + Y1**2) + SQR((X2-X5)**2 + (Y2-Y5)**2)))/(2*W1)
820 F4 = ((SQR((X1-X3)**2 + (Y1-Y3)**2) + SQR(Y2**2 +Y2**2)) -
         (SQR(X1**2 + Y1**2) + SQR((X2-X3)**2 + (Y2-Y3)**2)))/(2*W1)
840 F5 = ((SQR(X1**2 + Y1**2) + SQR((X2-X8)**2 + (Y2-Y8)**2)) -
         (SQR((X1-X8)**2 + (Y1-Y8)**2) + SQR(X2**2 + Y2**2)))/(2*W1)
860 F6 = ((SQR((X1-X5)**2 + (Y1-Y5)**2) + SQR((X2-X3)**2 + (Y2-Y3)**2)) -
         (SQR((X1-X2)**2 + (Y1-Y3)**2) + SQR((X2-X5)**2 + (Y2-Y5)**2)))/(2*W1)
890 IF X4>X7 THEN F7=F4 : GO TO 1060
900 U1 = X7 + W2*COS(T)
910 V1 = Y7 + W2*SIN(T)
920 IF U1>X3 THEN U1=X3 : V1=Y3
930 U1,V1 IS THE LOCATION OF THE UPPER EDGE OF THE UPPER SUN LIT BAND
940 F7 = 0: N = 0
950 F7 = F7 + ((SQR((X1-U1)**2 + (Y1-V1)**2) + SQR((X2-X3)**2 + (Y2-Y3)**2))
    -(SQR((X1-X7)**2 + (Y1-Y7)**2) + SQR((X2-U1)**2 + (Y2-V1)**2)))/(2*W1)
960 X7 = X7 - (W1 + W2)*COS(T)
970 Y7 = Y7 - (W1 + W2)*SIN(T)
980 U1 = X7 + W2*COS(T)
990 V1 = Y7 + W2*SIN(T)
995 ! X7,Y7 IS THE LOCATION OF THE LOWER EDGE OF THE SUN LIT BAND BEING CAL
      CULATED AND U1,V1 IS THE LOCATION OF THE UPPER EDGE OF THE SUN LIT BAND
      BEING CALCULATED.
```

```
1000 N = N + 1
1010 IF X7<0 THEN X7=0: Y7=0
1020 IF U1<0 GO TO 1060
1030 GO TO 950
1060 F8 = F4 - F7
1050 U2 = X6 + Y6/TAN(G)
1040 ! U2,0 IS THE LOCATION OF SHADOW PROJECTED BY THE LOWER EDGE OF THE
     LOWEST FIN ON THE PLANE OF THE ROOF.
1100 IF U2<=0 GO TO 1110
1105 F9 = F5 : GO TO 1170
1110 U3 = U2 + W1*COS(T)
1125 IF U3<0 THEN F9 = 0.5*F5 : GO TO 1170
1130 U4 = X6 + W1*COS(T)
1140 V4 = Y6 + W1*SIN(T)
1150 !U4,V4 IS THE LOCATION OF THE UPPER EDGE OF THE LOWEST FIN
1160 F9 = ((SQR((X1-U2)**2 + Y1**2) + SQR((X2-X8)**2 + Y2**2)) -
     (SQR((X2-U3)**2 + Y2**2) + SQR((X1-X8)**2 + Y1**2)))/(2*W1)
1170 F = F5 - F9
1200 M = ARC(SIN(D1)*SIN(L)*COS(T) - SIN(D1)*COS(L)*SIN(T) +
         (COS(D1)*COS(L)*COS(T) + COS(D1)*SIN(L)*SIN(T))*
         COS((12-K)*P/12)) ! ANGLE OF INCIDENCE
1210 E = 1353 + 44*COS(N1*P*2/365) ! BEAM INTENSITY OUTSIDE ATMOSPHERE
1220 E1 = E*R**(1/COS(Z2)) ! BEAM INTENSITY AT GROUND LEVEL
1230 E2 = E1*COS(M) ! INTENSITY ON FINS AND BACKING
1240 E3 = E1*COS(Z2) ! INTENSITY ON ROOF
1250 O1 = O1 + S2*A9*T1
1260 O2 = O2 + S2*F7*R1*A9*T1
1270 O3 = O3 + E3*(F9+F1)*R2*A9*T1
1280 O = O1 + O2 + O3
1290 NEXT K
1300 PRINT "DIRECT INPUT"2*O1"(WATT-HOURS/METER SQUARED)"
1310 PRINT "REFLECTED FROM BACKING"O2*2
1320 PRINT "REFLECTED FROM ROOF"O3*2
1330 PRINT "TOTAL INPUT"2*O
9999 END
```

Appendix C

MODELING PROGRAM SOLHP

Finds an iterative solution to heat pump pressure and temperature conditions; computes heat output and COP.

```
LIST
SDLHP   04:27 PM         25-Aug-81
2 DIM#1,F4(12,35),T4(12,2)
3 DIM Z9(35)
4!EVAPORATIVE HEAT EXCHANGER EQUATION
5 DEF FN0(T)=A*(B-T)
9!S2=CP FOR SATURATED VAPOR (BTU/LB*R, R)
10 DEF FNS2(T)=.124767+.461468E-4*T+.166926E-10*(T-300.)**4
19!S1=INTEGRAL CP*DT FOR LIQUID (BTU/LB, R)
20 DEF FNS1(T)=A5*T+A6*T*T+A7*T*T*T+A8*T**4
29!H2=ENTHALPY OF SATURATED VAPOR (BTU/LB., R)
30 DEFFNH2(T)=51.0186+.117806*T-.107586E-8*(T-300.)**4
39!H1= ENTHALPY OF LIQUID AT SATURATED CONDS. (BTU/LB, R)
40 DEFFNH1(T)=-97.9291+.229408*T+.314E-9*(T-150.)**4
49!P1= VAPOR PRESSURE (PSIA, R)
50 DEF FNP1(T)=B7*EXP(B8/T)*T**B9
55 READ Y4,Y5  !CRIT. GAS DENS.,CRIT. TEMP. (LBS./FT3, F.)
56 DATA 32.75,204.81
60 READ B7,B8,B9   !VAPOR PRESSURE CONSTANTS
61 DATA 1.0664E11,-5230.52,-1.69019
70 READ N1,N2,N3,N4,N5        !COMPRESSIBILITY CONSTANTS
71 DATA -1.47,1.183,1.2366,1.672,-.8083
80 READ R5,V0       !CLEARANCE FACTOR AND CFM OF COMPRESSOR
81 DATA .075,5
85 READ G0,G2                    !EVAP. AND COND. LUMPED CONDUCTANCES (W/F)
86 DATA 300,300
87 READ W0,W1,W2  !CURVE-FIT CONSTS. TO Q(EVAP), EQN IN F.
88 DATA 3185.8,73.724,.487473
89 READ T7,T8,T9 !FIRST AND SECOND SUCT. TEMP. GUESSES AND INITIAL
90!DISCH. TEMP. GUESS. T8 DECREMENT IS RELATIVE TO T7 RATHER THAN SRCE. TEMP.
91 DATA -20.,15.,20.
100 READ A5,A6,A7,A8  !CP*T FOR LIQUID
101 DATA .267165,8.96216E-6,-1.98675E-7,3.1145E-10
110 READ R9,W9          !RATIO OF CP TO CV AND FLUID MOL. WT.
111 DATA 1.19,86.47
120 READ E4,E5          !SUCTION AND DISCHARGE VALVE PRES. DROPS (PSI)
121 DATA 2.,2.
130 READ S3,S4          !SUCTION SUPER-HEAT PRIOR TO AND IN CYLINDER
131 DATA 10.,0.
140 READ S0,E1  !CONDENSATE SUB-COOL, DISCH. LINE TEMP. RETENTION
141 DATA 5.,1.
145 READ E7,E8          !NAMEPLATE HP. AND COMPRESSOR EFFICIENCY
146 DATA .3333,.9
148 Q7=746*E7*(1./(.562*E7**.201121*EXP(-9.229E-3*E7))-1.)
149 Y6=Y5+459.67
150 R4=1./R9:R8=1.-R4:R7=1.485/(W9*R8):R6=1.+R5:R3=10.73/W9
151 OPEN"SDL" AS FILE 1
152!:::::::::::::::
153 M=1
154!Q7=DISSIPATION OF CONVENTIONAL AC MOTOR OF E7 HORSEPOWER
155!H=COLLECTOR HT. TRANS. COEF.(W/M**2K),Z1=AIR TEMP. AMPLITUDE,Z0=MEAN AIR T.
156 H=10:Z1=2.4:Z0=42.5
157M2=T4(M,2)
158 FOR I=1 TO M2
159 Z9(I)=F4(M,1):NEXTI
160! END FIXED DATA INPUT**************************************************
```

```
161 A=845.4
165 Z=14(M,1)
166M1=1:M2=T4(M,2)
167 Y0=70.                          !BUILDING TEMP.  ***********======
169 S6=0.:S7=0.:S8=0.:S9=0.         !INITIALIZE ENERGY INTEGRALS
170 FOR I1=M1 TO MP          !INTEGRATION SPAN
171 Y3=Z1*SIN(.2618*Z-1.9635)+Z0
172 R=Y3+1.17*Z3(J1)/H              !AMBIENT/INSOLATION FACTOR FOR COLLECTOR
175 W2=Y3+T7:T0=Y0+T9
190 FOR J2=1 TO 10           !LOOP TO CALC. CONSISTENT EXCHGR./COMPRESSOR D
195 FOR J1=1 TO 10           !LOOP TO CALC. CONSISTENT SUCT./DISCH. TEMPS.
255 T3=W7:U0=T0+459.67:U1=U0-30:U3=T3+459.67:U4=U3+S3+S4:W4=U4-S4
270 H0=FNH1(U0):D1=FNS1(U0)-FNS1(U1):H3=FNH2(U3):D4=FNS2(U3)*(U4-U3)
280 P5=FNP1(U0)+E5:P4=FNP1(U3)-E4:P=P5/P4:P9=P**P8:U5=U4*P9
290 U6=U0*(1.-E1)+E1*U5
295 D5=R7*U4*(P9-1):D6=FNS2(U0)*(U5-U0):D7=FNS2(U3)*(W4-U3)
297!D1=TOTL. DISCH.,D2=D1-LOST S.H.,D3=TOTAL SUCT., D4=D3-S.H.(EVAP)
299 D1=H2-H0+D1+D4+D5:D2=D1-D6*(1.-E1)
300 D3=H3-H0+D1+D7:D4=D3-D7
301 !CALCULATE INTAKE STROKE VAPOR DENSITY
302 V1=U4/Y6:X2=X1*X1:R0=P4/(R3*U4*(4)
303 X3=N2/X2+N1/X1:X4=N3*(1-1/X2):R=R0:Z3=1
305 Z4=Z3:Z3=X3*R+X4*R*R+1.-(1.+N4*R+N5*R*R):R=R0/Z3
307 IF ABS(Z3-Z4)>.002 GO TO 305
320 F1=(P6-P5*P**R4)*R*Y4*V0
329 F=17.58*F1
330 D1=F*D1:D2=F*D2:D3=F*D3:D4=F*D4:D5=F*D5/E8
335 D6=D5+D7
336 C1=D1/D6:C2=(D1+D7+D5*(1.-E8))/D6:C3=D3/D6
340 T1=Y0+D2/B2
341 IF ABS(T1-T0)<.1 GO TO 350
345 T0=T1:NEXT J1
350 IF J2>1 GO TO 360
355 D8=D4-FND(T3):W8=T3:W7=T3+T8:GO TO 400
360 D9=D4-FND(T3):W9=T3
370 W=(D4*W9-D8*W8)/(D4-D8)
380 IF ABS(W-T3)<.1 GO TO 420
390 D8=D9:W7=W:W8=W
400 NEXT J2
420 T7=W-Y3:T9=T0-Y0          !USE SOLUTION TO CALC. MORE ACCURATE T7,T9
430 PRINT T0,Y0,Y3,W          !DISCH.,SINK,SRCE.,SUCT. TEMPS.
440 PRINT D1,D2,D3,D4,D5      !COND-TOTL.,COND/PARTIAL S.H.,EV-TOTL.,EV-SATD.,EV
450 PRINT D6,D7,C1,C2,C3      !ELEC. MOTOR,MOTOR DISS.,COP-COND-TOT.,COP-COND
451!WITH CREDIT FOR MOTOR AND COMP. FRICT.,COP-EVAP-TOT.
455 PRINT
490 S9=S9+.5*D6:S8=.5*D6              !TOTAL ELEC. MOTOR INPUT
495 S7=S7+S6+.5*C2*D6:S6=.5*C2*D6      !TOTAL HEAT OUTPUT (W-HRS)
500 Z=Z+.5:NEXT I1                     !HALF-HOUR TIME INCREMENTS
530 S9=15.*S9:S7=15.*S7
550 PRINT"ELEC. INPUT, HEAT OUTPUT,COP, DIFFERENCE=";S9,S7,S7/S9,S7-S9
900 CLOSE 1
1000 END

READY

OLD SUN

READY
```


* U.S. GOVERNMENT PRINTING OFFICE: 1982-646-069/210